IOPscience iopscience.iop.org

Home Search Collections Journals About Contact us My IOPscience

Josephson φ-junctions based on structures with complex normal/ferromagnet bilayer

This content has been downloaded from IOPscience. Please scroll down to see the full text.

2013 Supercond. Sci. Technol. 26 015005

(http://iopscience.iop.org/0953-2048/26/1/015005)

View the table of contents for this issue, or go to the journal homepage for more

Download details:

IP Address: 130.89.45.232
This content was downloaded on 20/04/2016 at 09:54

Please note that terms and conditions apply.

Supercond. Sci. Technol. **26** (2013) 015005 (15pp) doi:10.1088/0953-2048/26/1/015005

Josephson φ-junctions based on structures with complex normal/ferromagnet bilayer

S V Bakurskiy[1,2], N V Klenov[1], T Yu Karminskaya[2], M Yu Kupriyanov[2] and A A Golubov[3]

[1] Faculty of Physics, Lomonosov Moscow State University, Leninskie Gory, Moscow 119991, Russian Federation
[2] Skobeltsyn Institute of Nuclear Physics, Lomonosov Moscow State University 1(2), Leninskie Gory, Moscow 119991, Russian Federation
[3] Faculty of Science and Technology and MESA+ Institute for Nanotechnology, University of Twente, 7500 AE Enschede, The Netherlands

E-mail: r3zz@mail.ru (S V Bakurskiy)

Received 28 August 2012, in final form 17 October 2012
Published 14 November 2012
Online at stacks.iop.org/SUST/26/015005

Abstract
We demonstrate that Josephson devices with a nontrivial phase difference $0 < \varphi_g < \pi$ in the ground state can be realized in structures composed of longitudinally oriented normal metal (N) and ferromagnet (F) films in the weak link region. Oscillatory coupling across the F-layer makes the first harmonic in the current–phase relation relatively small, while coupling across the N-layer provides a negative sign of the second harmonic. To derive quantitative criteria for a φ-junction, we have solved the two-dimensional boundary-value problem in the frame of Usadel equations for overlap and ramp geometries of S–NF–S structures. Our numerical estimates show that φ-junctions can be fabricated using up-to-date technology.

(Some figures may appear in colour only in the online journal)

1. Introduction

The relation between the supercurrent I_S across a Josephson junction and the phase difference φ between the phases of the order parameters of superconducting (S) banks is an important characteristic of a Josephson structure [1, 2]. In standard SIS structures with the tunnel type of conductivity of a weak link, the current–phase relation (CPR) has the sinusoidal form $I_S(\varphi) = A\sin(\varphi)$. On the other hand, in SNS or SINIS junctions with a metallic type of conductivity, the smaller the temperature T, the larger the deviations from the $\sin(\varphi)$ form [1], and $I_S(\varphi)$ achieves its maximum at $\pi/2 \leq \varphi \leq \pi$. In SIS junctions the amplitude B of the second harmonic in the CPR, $B\sin(2\varphi)$, is of second order in the transmission coefficient of the tunnel barrier I and therefore negligibly small for all T. In SNS structures the second CPR harmonic is also small in the vicinity of the critical temperature T_C of superconductors, where $A \sim (T_C - T)$. At low temperatures $T \ll T_C$, the coefficients A and B have comparable magnitudes, thus giving rise to qualitative modifications of the shape of the CPR with a decrease of T.

It is important to note that in all the types of junctions discussed above the ground state is achieved at $\varphi = 0$, since at $\varphi = \pi$ a junction is in a non-equilibrium state.

The situation changes in Josephson structures involving ferromagnets as weak link materials. The possibility of the so-called 'π -state' in SFS Josephson junctions (characterized by the negative sign of the critical current I_C) has been predicted theoretically and observed experimentally [2–29]. In contrast to traditional Josephson structures, in SFS devices it is possible to have the ground state $\varphi_g = \pi$ (so-called π-junctions), while $\varphi = 0$ corresponds to an unstable situation. It was proved experimentally [30, 31] that π-junctions can be used as on-chip π-phase shifters or π-batteries for self-biasing various electronic quantum and classical circuits. It was proposed to use π self-biasing to decouple quantum circuits from the environment or to replace conventional inductances and greatly reduce the size of an elementary cell [32].

 © 2013 IOP Publishing Ltd Printed in the UK & the USA

In some classical and quantum Josephson circuits it is even more interesting to create on-chip φ-batteries. They are φ-junctions, the structures having phase difference $\varphi_g = \varphi$, $(0 < |\varphi| < \pi)$ between superconducting electrodes in the ground state. The φ-states were first predicted by Mints [33] for the case of randomly distributed alternating 0- and π-Josephson junctions along grain boundaries in high-T_c cuprates with d-wave order parameter symmetry. It was shown later that φ-junctions can be also realized in a periodic array of 0 and π SFS junctions [34, 35]. It was demonstrated that depending on the length of 0 or π segments in the array, a modulated state with the average phase difference φ_g can be generated if the mismatch length between the segments is small. This φ_g can take any value within the interval $-\pi \leq \varphi_g \leq \pi$. The constraints on parameter spread of individual segments in such arrays were estimated in [36]. Recently, remarkable progress was achieved in realization of φ-junctions consisting of only two parallel elements: 0 and π regions of different lengths [37–39]. Such junctions were fabricated on the basis of Nb/CuNi heterostructures, they have moderate normalized lengths and are magnetically tunable. Recently φ-states were predicted in junctions between conventional superconductors and iron pnictides. [40].

In general, in order to implement a φ-junction one has use a Josephson junction having a non-sinusoidal current–phase relation, which, at least, can be described by a sum of two terms

$$I_S(\varphi) = A\sin(\varphi) + B\sin(2\varphi). \quad (1)$$

Moreover, the following special relationship between the amplitudes of the harmonics of the CPR, A and B, is needed for existence of an equilibrium stable state [41, 42]

$$|B| > |A|/2, \qquad B < 0. \quad (2)$$

In conventional junctions, the magnitude of A is larger than that of B and the inequalities (2) are difficult to fulfil. However, in SFS junctions in the vicinity of the 0 to π transition the amplitude of the first harmonic in the CPR is close to zero, thus opening an opportunity for making a φ-battery, if B can be made negative. It is well known that SFS junctions with a metallic type of conductivity, as well as SIFS structures [43, 44] with high transparencies of SF interfaces, have a complex decay length of superconducting correlations induced into the F-layer $\xi_H = \xi_1 + i\xi_2$. Unfortunately, the conditions (2) are violated in these types of junctions due to the following dependence of coefficients A, B on the junction length L: $A \sim \exp\{-L/\xi_1\}\cos(L/\xi_2)$, $B \sim -\exp\{-2L/\xi_1\}\cos(2L/\xi_2)$. As a result, the coefficient B is positive for $L = (\pi/2)\xi_2$ corresponding to the first 0 to π transition.

Quantitative calculations made in the framework of microscopic theory [45, 46] confirm the above qualitative analysis. In [45, 46] it was demonstrated that in SFS sandwiches with either clean or dirty ferromagnetic metal interlayers the transition from the 0 to π state is of first order, that is $B > 0$ at any transition point [3].

It was suggested recently in [47–52] to fabricate 'current in plane' SFS devices having a weak link region consisting of NF or FNF multilayers with the supercurrent flowing parallel to the FN interfaces. In these structures, superconductivity is induced from the S banks into the normal (N) film, while F films serve as a source of spin-polarized electrons, which diffuse from the F-layer to the N-layer, thus providing an effective exchange field in a weak link. Its strength can be controlled [53, 54] by transparencies of NF interfaces, as well as by the products of densities of states at the Fermi level, N_F, N_N, and film thicknesses, d_F, d_N . It was shown in [47–51] that the reduction of effective exchange energy in a weak link permits one to increase the decay length from the scale of the order of ∼1 up to ∼100 nm. The calculations performed in these papers did not go beyond a linear approximation in which the amplitude of the second harmonic in the CPR is small. Therefore, the question of the feasibility of φ-contacts in these structures has not been studied and remains open to date.

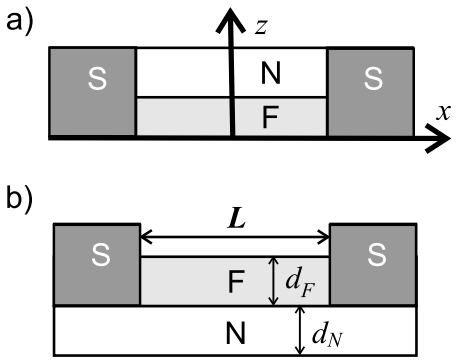

Figure 1. (a) The S–NF–S junction in the ramp-type geometry and (b) the SN–FN–NS junction in the ramp-type overlap (RTO) geometry.

The purpose of this paper is to demonstrate that the same 'current in plane' devices (see figure 1) can be used as effective φ-shifters. The structure of the paper is as follows. In section 2 we present a general qualitative discussion of the microscopic mechanisms leading to formation of higher harmonics in the CPR. In section 3 we formulate a quantitative approach in terms of the Usadel equations. In section 4 the criteria of φ-state existence are derived for a ramp-type S–FN–S structure. Section 5 shows the advantage of the other geometries in order to realize the φ-state. Finally, in section 6 we consider properties of real materials and estimate the possibility to realize φ-states using up-to-date technology.

2. CPR formation mechanisms

In this section we shall discuss microscopic processes which contribute to the formation of the CPR in Josephson junctions. We will show that in junctions with a normal interlayer the coefficient A in equation (1) is positive and the coefficient B is negative, while in SFS junctions the coefficient B becomes positive near the point of the 0 to π transition.

The physical reason leading to the sign reversal of the coefficient B in SFS junctions compared to that in SNS structures can be understood from the simple diagram shown in figure 2, illustrating the mechanisms of supercurrent

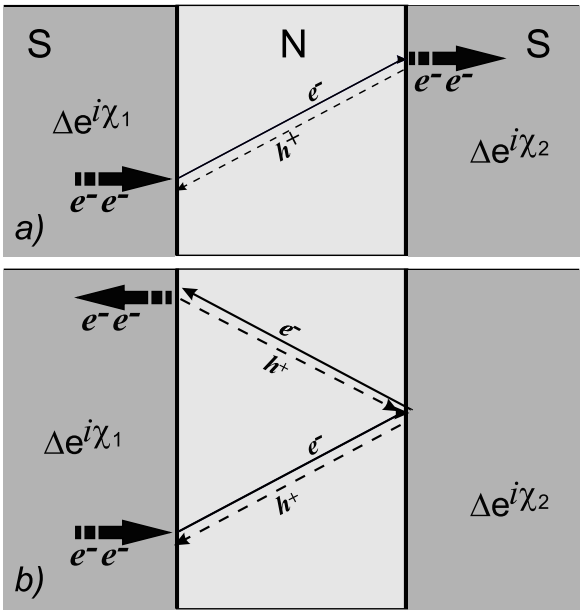

Figure 2. Diagrams of the processes forming the first (a) and second (b) harmonics of the CPR in the SNS and SFS structures.

transfer in double-barrier Josephson junctions. Consider an electron-like quasiparticle e^- propagating across a SINIS structure towards the right electrode. This quasiparticle can be reflected either in the Andreev or in the normal channel.

The result of the first process (see figure 2(a)) is generation in the weak link region (with an amplitude proportional to $\exp(\mathrm{i}\chi_2)$) of the hole h^+ propagating in the opposite direction. Andreev reflection of this hole at the second interface (with an amplitude proportional to $\exp(-\mathrm{i}\chi_1)$) results in transfer of a Cooper pair from the left to the right electrode with a rate proportional to the net coefficient of Andreev reflection processes [55, 56] at both SN interfaces, $AR(\varphi) = \alpha(\varphi)\exp(\mathrm{i}\varphi)$, $\varphi = (\chi_2 - \chi_1)$. The amplitude, $\alpha(\varphi)$, depends on the geometry of the structure and on material parameters. Note that for given values of these parameters $\alpha(\varphi) = \alpha(-\varphi)$, according to the detailed balance relations [55]. Similar considerations show that a quasiparticle e^- moving towards the left electrode generates a Cooper pair propagating from the right to the left interface with a rate proportional to $AR(-\varphi) = \alpha(\varphi)\exp(-\mathrm{i}\varphi)$. The difference between the two processes described above determines a supercurrent I_S, which is proportional to $\sin(\varphi)$.

The result of the second process is the change (with an amplitude proportional to $\exp(\mathrm{i}\chi_2)$) of the e^- propagation direction to the left electrode and nucleation of a Cooper pair and a hole propagating to the right electrode (with an amplitude proportional to $\exp(-\mathrm{i}\varphi)$). After normal reflection from the right interface (with an amplitude proportional to $\exp(\mathrm{i}\chi_2)$) the hole arrives at the left SN interface and closes this Andreev loop by generating a Cooper pair in the left electrode and an electronic state (with an amplitude proportional to $\exp(-\mathrm{i}\chi_1)$). The Cooper pair has to undergo a full reflection at the SN interface, thus again a pair is generated moving in the direction opposite to that in the main Andreev loop. The net coefficient of this Andreev reflection process is $BR(\varphi) = \beta(\varphi)\exp(2\mathrm{i}\varphi)$. For a quasiparticle e^- moving in the weak link towards the left electrode the same consideration leads to generation of two Cooper pairs moving from the left to the right with a rate proportional to $BR(-\varphi) = \beta(\varphi)\exp(-2\mathrm{i}\varphi)$. The difference between these two processes determines a part of the supercurrent I_S proportional to $\sin(2\varphi)$.

As follows from the above arguments, in junctions with a normal interlayer supercurrent, components proportional to $\sin(\varphi)$ and $\sin(2\varphi)$ have opposite signs, and the coefficient B in equation (1) is negative. This statement is in full agreement with calculations of the CPR performed in the frame of the microscopic theory of superconductivity [1, 2]. It is valid if a supercurrent across a junction does not suppress superconductivity in S electrodes in the vicinity of SN interfaces [57–59]. In addition, an effective path of the particles in the second process discussed above is two times larger than in the first one. This leads to stronger decay of the second harmonic amplitude B with increasing distance L.

In SFS junctions the situation becomes more complicated. The exchange field, H, in the weak link removes the spin degeneracy of the quasiparticles. As a result, one has to consider four types of Andreev loops instead of the two loops discussed above. One should also take into account the fact that the wave function of a quasiparticle propagating through the weak link acquires an additional phase shift φ_H proportional to the magnitude of the exchange field [60]. The sign of φ_H depends on the mutual orientations between magnetization of the ferromagnetic film and the spin of a quasiparticle. Taking into account these phase shifts and repeating arguments similar to given above, one can show that the coefficients A and B in equation (1) acquire additional factors $\cos(2\varphi_H)$ and $\cos(4\varphi_H)$, respectively. At the point of the 0 to π transition the coefficient $A = 0$, that is $\varphi_H = \pi/4$. As a result, $\cos(4\varphi_H)$ provides an additional factor which changes the sign of the second harmonic amplitude B in SFS structures from negative to positive.

In the present study we will show that, in contrast to SFS devices with a standard geometry, it is possible to realize φ-junctions in the structures shown in figure 1. Qualitatively, these structures are superpositions of parallel SNS and SFS channels, where the supercurrent $I_S(\varphi)$ can be decomposed into two parts, $I_N(\varphi)$ and $I_F(\varphi)$, flowing across N and F films, respectively. For $L \ll \xi_N$ and at sufficiently low temperatures $I_N(\varphi)$ has a large negative second CPR harmonic B_N. For $L > \xi_1$ the supercurrent in the SFS-channel exhibits damped oscillations as a function of L. In this regime the second harmonic of the CPR is negligibly small compared to the first one. The large difference between the decay lengths of superconducting correlations in N and F materials allows one to enter the regime when $\xi_1 < L < \xi_N$. In this case the first CPR harmonic $A = A_N + A_F$ can be made small enough due to the negative sign of A_F, while the second CPR harmonic $B \approx B_N$ is negative, thus making it possible to fulfil the condition (2). Note that we are considering here the regime of finite interface transparencies, when higher-order harmonics decay fast with the harmonic order. Therefore, it is sufficient to consider only the first and second harmonics of the CPR in all our subsequent discussions.

We show below that the mechanism described above indeed works in the considered S–FN–S junctions, and we estimate the corresponding parameter range when φ-states can be realized.

3. Model

We consider two types of symmetric multilayered structures shown schematically on figure 1. The structures consist of a superconducting (S) electrode contacting either the end-wall of a FN bilayer (ramp-type junctions) or the surface of F or N films (overlap junction geometry). The FN bilayer consists of ferromagnetic (F) film and normal metal (N) having thicknesses d_F, and d_N respectively. We suppose that the conditions of a dirty limit are fulfilled for all metals and that the effective electron–phonon coupling constant is zero in the F and N films. For simplicity we assume that the parameters γ_{BN} and γ_{BF}, which characterize the transparencies of NS and FS interfaces,

$$\gamma_{BN} = \frac{R_{BN}\mathcal{A}_{BN}}{\rho_N\xi_N} \gg \frac{\rho_S\xi_S}{\rho_N\xi_N}, \qquad \gamma_{BF} = \frac{R_{BF}\mathcal{A}_{BF}}{\rho_F\xi_F} \gg \frac{\rho_S\xi_S}{\rho_F\xi_F}, \tag{3}$$

are large enough in order to neglect suppression of superconductivity in the S parts of the junctions. Here R_{BN}, R_{BF}, $\mathcal{A}_{BN}$ and $\mathcal{A}_{BF}$ are the resistances and areas of the SN and SF interfaces, ξ_S, ξ_N and ξ_F are the decay lengths of S, N and F materials and ρ_S, ρ_N and ρ_F are their resistivities.

Under the above conditions the problem of calculating the supercurrent in the structures reduces to solution of the set of Usadel equations [3, 4, 61]

$$\frac{\xi^2}{G_\omega}\left[\frac{\partial}{\partial x}\left[G_\omega^2\frac{\partial}{\partial x}\Phi_\omega\right]+\frac{\partial}{\partial z}\left[G_\omega^2\frac{\partial}{\partial z}\Phi_\omega\right]\right]-\frac{\tilde\omega}{\pi T_C}\Phi_\omega=0, \qquad G_\omega=\frac{\tilde\omega}{\sqrt{\tilde\omega^2+\Phi_\omega\Phi^*_{-\omega}}}, \tag{4}$$

where Φ_ω and G_ω are Usadel Green's functions in Φ parametrization. They are $\Phi_{\omega,N}$ and $G_{\omega,N}$ or $\Phi_{\omega,F}$ and $G_{\omega,F}$ in the N and F films respectively, $\omega = \pi T(2m+1)$ are Matsubara frequencies ($m = 0, 1, 2, \ldots$), $\tilde\omega = \omega + iH$, H is the exchange field of the ferromagnetic material, $\xi^2 = \xi^2_{N,F} = D_{N,F}/2\pi T_C$ for the N-layer and F-layer respectively, and $D_{N,F}$ are diffusion coefficients. To write equations (4), we have chosen the z and x axis, respectively, in directions perpendicular and parallel to the plane of the N film and we have set the origin in the middle of structure at the free interface of the F film (see figure 1).

The supercurrent $I_S(\varphi)$ can be calculated by integrating the standard expressions for the current density $j_{N,F}(\varphi, z)$ over the junction cross-section:

$$\frac{2ej_{N,F}(\varphi,z)}{\pi T} = \sum_{\omega=-\infty}^{\infty}\frac{iG_\omega^2}{\rho_{N,F}\tilde\omega^2_{N,F}}\left[\Phi_\omega\frac{\partial\Phi^*_{-\omega}}{\partial x}-\Phi^*_{-\omega}\frac{\partial\Phi_\omega}{\partial x}\right], \tag{5}$$

$$I_S(\varphi) = W\int_0^{d_F} j_F(\varphi,z)\,dz + W\int_{d_F}^{d_F+d_N} j_N(\varphi,z)W\,dz,$$

where W is the width of the junctions, which is supposed to be small compared to the Josephson penetration depth. It is convenient to perform the integration in (5) in the F-layer and N-layer separately along the line located at $x = 0$, where the z-component of the supercurrent density vanishes by symmetry.

Equation (4) must be supplemented by the boundary conditions [62]. Since these conditions link the Usadel Green's functions corresponding to the same Matsubara frequency ω, we may simplify the notations by omitting the subscript ω. At the NF interface the boundary conditions have the form

$$\gamma_{BFN}\xi_F\frac{\partial\Phi_F}{\partial z} = -\frac{G_N}{G_F}\left(\Phi_F-\frac{\tilde\omega}{\omega}\Phi_N\right), \qquad \gamma_{BNF}\xi_N\frac{\partial\Phi_N}{\partial z} = \frac{G_F}{G_N}\left(\Phi_N-\frac{\omega}{\tilde\omega}\Phi_F\right), \qquad \gamma_{BFN} = \frac{R_{BFN}\mathcal{A}_{BFN}}{\rho_F\xi_F} = \gamma_{BNF}\frac{\rho_F\xi_F}{\rho_N\xi_N}, \tag{6}$$

where R_{BFN} and $\mathcal{A}_{BFN}$ are the resistance and area of the NF interface.

The conditions at free interfaces are

$$\frac{\partial\Phi_N}{\partial n} = 0, \qquad \frac{\partial\Phi_F}{\partial n} = 0. \tag{7}$$

The partial derivatives in (7) are taken in the direction normal to the boundary, so that n can be either z or x depending on the particular geometry of the structure.

In writing the boundary conditions at the interface with a superconductor, we must take into account the fact that in our model we have ignored the suppression of superconductivity in electrodes, so that in the superconductor

$$\Phi_S(\pm L/2) = \Delta\exp(\pm i\varphi/2), \qquad G_S = \frac{\omega}{\sqrt{\omega^2+\Delta^2}}, \tag{8}$$

where Δ is the magnitude of the order parameter in S banks. Therefore for NS and FS interfaces we may write

$$\gamma_{BN}\xi_N\frac{\partial\Phi_N}{\partial n} = \frac{G_S}{G_N}(\Phi_N-\Phi_S(\pm L/2)), \tag{9a}$$

$$\gamma_{BF}\xi_F\frac{\partial\Phi_F}{\partial n} = \frac{G_S}{G_F}\left(\Phi_F-\frac{\tilde\omega}{\omega}\Phi_S(\pm L/2)\right). \tag{9b}$$

As in equation (7), n in equations (9*a*) and (9*b*) is a normal vector directed into the material marked at the derivative.

For the structure presented in figure 1(a), the boundary-value problem (4)–(9*b*) was solved analytically in the linear approximation [50, 51], i.e. under conditions

$$G_N \equiv \mathrm{sgn}(\omega), \qquad G_F \equiv \mathrm{sgn}(\omega). \tag{10}$$

In the present study we will go beyond the linear approximation where qualitatively new effects are found.

4. Ramp-type geometry

The ramp-type Josephson junction has the simplest geometry among the structures shown in figure 1. It consists of the NF

bilayer, laterally connected with superconducting electrodes (see figure 1(a)).

In general, there are three characteristic decay lengths in the considered structure [47, 50, 71]. They are ξ_N, $\xi_H = \xi_1 + i\xi_2$ and $\zeta = \zeta_1 + i\zeta_2$. The first two lengths determine the decay and oscillations of superconducting correlations far from the FN interface, while the last one describes their behavior in its vicinity. A similar length scale ζ occurs in a vicinity of a domain wall [63–71]. In the latter, the exchange field is averaged out for antiparallel directions of magnetizations, and the decay length of superconducting correlations becomes close to ξ_N. At the FN interface, the flow of spin-polarized electrons from F to N metal and reverse flow of unpolarized electrons from N to F suppresses the exchange field in its vicinity to a value smaller than that in a bulk ferromagnetic material, thus providing the existence of ζ. Under a certain set of parameters [47] these lengths, ζ_1 and ζ_2, can become comparable to ξ_N, which is typically much larger than ξ_1 and ξ_2, which are equal to $\xi_F\sqrt{\pi T_C/H}$ for $H \gg \pi T_C$.

The existence of three decay lengths, ξ_N, ζ and ξ_H, should lead to the appearance of three contributions to the total supercurrent, I_N, I_{FN} and I_F, respectively. The main contribution to the I_N component comes from a part of the supercurrent uniformly distributed in a normal film. In accordance with the qualitative analysis carried out in section 2, it is the only current component which provides a negative value of the amplitude of the second harmonic B in the current–phase relation. The smaller the distance between electrodes, L, the larger this contribution. To realize a φ-contact, one must compensate for the amplitude of the first harmonic, A, in a total current to a value that satisfies the requirement (2). The contribution to A from I_N also increases with decreasing L. Obviously, it is difficult to suppress the coefficient A due to the I_{FN} contribution only, since I_{FN} flows through thin near-boundary layer. Therefore, the strong reduction of A required to satisfy the inequality (2) can only be achieved as a result of compensation of the currents I_N and I_F flowing in opposite directions in N and F films far from the FN interface. Note that the oscillatory nature of the $I_F(L)$ dependence allows us to satisfy requirement (2) in a certain range of L. The role of I_{FN} in a balance between I_N and I_F can be understood by solving the boundary-value problem (4)–(9*b*), which admits an analytic solution in some limiting cases.

4.1. Limit of small L

The solution of the boundary-value problem (4)–(9*b*) can be simplified in the limit of a small distance between superconducting electrodes

$$L \ll \min\{\xi_1, \xi_N\}. \tag{11}$$

In this case one can neglect non-gradient terms in (4) and obtain that contributions to the total current resulting from the redistribution of currents near the FN interface cancel each other, leading to $I_{FN} = 0$ (see appendix A for the details). As a result, the total current $I_S(\varphi)$ is a sum of two terms only

$$I_S(\varphi) = I_N(\varphi) + I_F(\varphi),$$
$$\frac{2eI_N(\varphi)}{\pi TWd_N} = \frac{1}{\gamma_{BN}\xi_N\rho_N}\sum_{\omega=-\infty}^{\infty}\frac{\Delta^2 G_N G_S \sin(\varphi)}{\omega^2}, \tag{12}$$

$$\frac{2eI_F(\varphi)}{\pi TWd_F} = \frac{1}{\gamma_{BF}\xi_F\rho_F}\sum_{\omega=-\infty}^{\infty}\frac{\Delta^2 G_N G_S \sin(\varphi)}{\omega^2}, \tag{13}$$

where $G_N = \frac{\omega}{\sqrt{\omega^2+\Delta^2\cos^2(\frac{\varphi}{2})}}$. The currents $I_N(\varphi)$ and $I_F(\varphi)$ flow independently across the F and N parts of the weak link. The $I_{N,F}(\varphi)$ dependences coincide with those calculated previously for double-barrier junctions [62] in the case when L lies within the interval defined by the inequalities (11).

It follows from (12), (13) that in the considered limit neither the presence of a sharp FN boundary in the weak link region, nor the strong difference in transparencies of SN and SF interfaces, lead to intermixing of the supercurrents flowing in the F and N channels. It is also seen that the amplitude of the first harmonic of the $I_F(\varphi)$ current component is always positive and the requirement (2) cannot be achieved.

4.2. Limit of intermediate L

For intermediate values of spacing between the S electrodes

$$\xi_1 \ll L \ll \xi_N \tag{14}$$

and for values of suppression parameters at SN and SF interfaces satisfying the conditions (3), the boundary problem (4)–(9*b*) can be solved analytically for a sufficiently large magnitude of suppression parameter γ_{BFN}. It is shown in appendix B that under these restrictions in the first approximation we can neglect the suppression of superconductivity in the N film due to proximity with the F-layer and find that

$$\Phi_N = \Delta\cos\left(\frac{\varphi}{2}\right) + i\frac{\Delta G_S \sin\left(\frac{\varphi}{2}\right)}{\gamma_{BN}G_N}\frac{x}{\xi_N},$$
$$G_N = \frac{\omega}{\sqrt{\omega^2 + \Delta^2\cos^2(\frac{\varphi}{2})}}, \tag{15}$$

while the spatial distribution of $\Phi_F(x, z)$ includes three terms: the first two describe the influence of the N film, while the last one has the form well known for SFS junctions [2–4].

Substitution of these solutions into the expression for the supercurrent (5) leads to a $I_S(\varphi)$ dependence consisting of three terms

$$I_S(\varphi) = I_N(\varphi) + I_F(\varphi) + I_{FN}(\varphi). \tag{16}$$

Here $I_N(\varphi)$ is the supercurrent across the N-layer. In the considered approximation $I_N(\varphi)$ is given by the expression (12). The second term in (16) equals the supercurrent across the SFS double-barrier structure in the limit of small transparencies of SF interfaces [72, 73]

$$\frac{2eI_F(\varphi)}{\pi TWd_F} = \frac{\Delta^2\sin(\varphi)}{\gamma_{BF}^2\xi_F\rho_F}\sum_{\omega=-\infty}^{\infty}\frac{G_S^2}{\omega^2\sqrt{\tilde{\Omega}}\sinh(2q_L)}, \tag{17}$$

where $q_L = L\sqrt{\tilde{\Omega}}/2\xi_F$, $\tilde{\Omega} = |\Omega| + iH\mathrm{sgn}(\Omega)/\pi T_C$, $\Omega = \omega/\pi T_C$.

The last contribution is shown in appendix B to contain three components

$$I_{FN}(\varphi) = I_{FN1}(\varphi) + I_{FN2}(\varphi) + I_{FN3}(\varphi) \tag{18}$$

with additional smallness parameters γ_{BFN}^{-1} and $\gamma_{BFN}^{-1}\xi_F/\xi_N$ compared to the current $I_F(\varphi)$ given by equation (17). Nevertheless, these currents should be taken into account in the analysis because they decay significantly slower than $I_F(\varphi)$ with increasing L.

4.3. φ-state existence

The conditions for the implementation of a φ-contact are better, the larger the relative amplitude of the second harmonic, which increases at low temperatures. Therefore, low-temperature regime is most favorable for a φ-state. In the limit $T \ll T_C$ we can go from summation to integration over ω in (12), (17), (B.15)–(B.17). From (12) we have

$$\frac{2eI_N(\varphi)}{Wd_N} = \frac{\Delta}{\gamma_{BN}\xi_N\rho_N} K\left(\sin\frac{\varphi}{2}\right)\sin(\varphi), \tag{19}$$

where $K(x)$ is the complete elliptic integral of the first kind. Expanding expression (19) in a Fourier series it is easy to obtain

$$A_N = Q_0\frac{8}{\pi}\int_0^1 x^2\sqrt{1-x^2}K(x)\,dx = \Upsilon_A Q_0, \tag{20}$$

$$B_N = 2A_N - \frac{32}{\pi}Q_0\int_0^1 x^4\sqrt{1-x^2}K(x)\,dx = \Upsilon_B Q_0, \tag{21}$$

where $Q_0 = \Delta W d_N/e\gamma_{BN}\xi_N\rho_N$, A_N, B_N are the first and the second harmonic amplitudes of $I_N(\varphi)$, and

$$\Upsilon_A = \frac{2\pi^2}{\Gamma^2(-\frac{1}{4})\Gamma^2(\frac{7}{4})} \simeq 0.973,$$

$$\Upsilon_B = 2\Upsilon_A - \frac{\pi}{2^3}F_2\left(\frac{1}{2},\frac{1}{2},\frac{5}{2};1,4;1\right) \simeq -0.146,$$

where $\Gamma(z)$ is the Gamma function and ${}_pF_q$ is the generalized hypergeometric function.

Evaluation of the sums in (17), (B.15)–(B.17) can be done for $H \gg \pi T_C$ and $T \ll T_C$, resulting in $I_F(\varphi) = A_F\sin(\varphi)$ with

$$A_F = P_0\frac{2}{\sqrt{h}}\exp(-\kappa L)\cos\left(\kappa L + \frac{\pi}{4}\right), \tag{22}$$

$\kappa = \sqrt{h}/\sqrt{2}\xi_F$, $h = H/\pi T_C$ and $P_0 = \Delta W d_F/e\gamma_{BF}^2\xi_F\rho_F$. Substitution of (20) and (21) into the inequalities (2) gives φ-state requirements for ramp-type structure

$$\left|\Upsilon_A + \frac{1}{\varepsilon}\Psi(L)\right| < 2|\Upsilon_B|, \qquad \varepsilon = \frac{\sqrt{h}\gamma_{BF}^2}{2\gamma_{BN}}\frac{d_N\xi_F\rho_F}{d_F\xi_N\rho_N}, \tag{23}$$

$$\Psi(L) = \exp(-\kappa L)\cos\left(\kappa L + \frac{\pi}{4}\right).$$

This expression gives the limitation on geometrical and material parameters of the considered structures, providing the existence of the φ-junction. Function $\Psi(L)$ has the first minimum at $\kappa L = \pi/2$, $\Psi(\pi/2\kappa) \approx -0.147$.

It is convenient to formulate the conditions for the realization of φ-junctions in terms of the dimensionless parameter ε introduced in equation (23), as will be done below in this paper.

For large values of ε, inequality (23) cannot be fulfilled at any length L. Thus solutions exist only in the area with upper limit

$$\varepsilon < \frac{-\Psi(\pi/2\kappa)}{\Upsilon_A - 2|\Upsilon_B|} \approx 0.216. \tag{24}$$

At $\varepsilon \approx 0.216$ the left-hand side of inequality (23) equals its right-hand part, providing the nucleation of an interval of κL in which we can expect the formation of a φ-contact. This interval increases with a decrease of ε and achieves its maximum length

$$1.00 \lesssim \kappa L \lesssim 2.52, \tag{25}$$

at $\varepsilon = \frac{-\Psi(\pi/2\kappa)}{\Upsilon_A + 2|\Upsilon_B|} \approx 0.116$. It is necessary to note that at $\varepsilon = -\Psi(\pi/2\kappa)/\Upsilon_A \approx 0.151$ there is a transformation of the left-hand side local minimum in (23), which occurs at $\kappa L = \pi/2$, into a local maximum; so that at $\varepsilon \approx 0.116$ both sides of (23) become equal to each other, and the interval (25) of φ-junction existence subdivides into two parts. With a further decrease of ε, these parts are transformed into narrow bands, which are localized in the vicinity of the 0 to π transition point ($A_N + A_F = 0$); they take place at $\kappa L = \pi/4$ and $\kappa L = 5\pi/4$. The widths of the bands decrease with a decrease of ε.

Thus, our analysis has shown that for

$$0.12 \lesssim \varepsilon \lesssim 0.2 \tag{26}$$

we can expect the formation of a φ-junction in a sufficiently wide range of distances ΔL between the electrodes determined by (23). Now we will take into the account the impact of the interface term $I_{FN}(\varphi)$. In the considered approximations, it follows from (B.15) to (B.17) that

$$I_{FN1}(\varphi) = \frac{2U_0\xi_F\exp(-\frac{\kappa L}{2})\cos(\frac{\kappa L}{2}-\frac{\pi}{4})}{\gamma_{BF}\gamma_{BN}\xi_N h^{3/2}}\sin(\varphi), \tag{27}$$

$$I_{FN2}(\varphi) = -\frac{\sqrt{2}U_0\xi_F}{4h^{3/2}\gamma_{BN}\gamma_{BFN}\xi_N}\sin(\varphi)K\left(\sin\frac{\varphi}{2}\right), \tag{28}$$

$$I_{FN3}(\varphi) = -\frac{2U_0\exp(-\frac{\kappa L}{2})\sin(\frac{\kappa L}{2})}{h\gamma_{BF}}\sin(\varphi)K\left(\sin\frac{\varphi}{2}\right), \tag{29}$$

where $U_0 = \Delta W/e\gamma_{BFN}\rho_F$. In the range of distances between the electrodes $\pi/4 < \kappa L < 5\pi/4$ currents $I_{FN2}(\varphi)$ and $I_{FN3}(\varphi)$ are negative. These contributions have the same form of the CPR as it is for the $I_N(\varphi)$ term, and due to negative sign suppress the magnitude of supercurrent across the junction, thus making the inequality (23) easier to satisfy. The requirement $B < 0$ imposes an additional restriction on the value of the suppression parameter γ_{BFN}

$$\gamma_{BFN} > \frac{\rho_N\xi_N}{hd_N\rho_F}\left(\frac{\xi_F}{\xi_N\gamma_{BFN}h^{1/2}} + \frac{\gamma_{BN}}{\gamma_{BF}}\right). \tag{30}$$

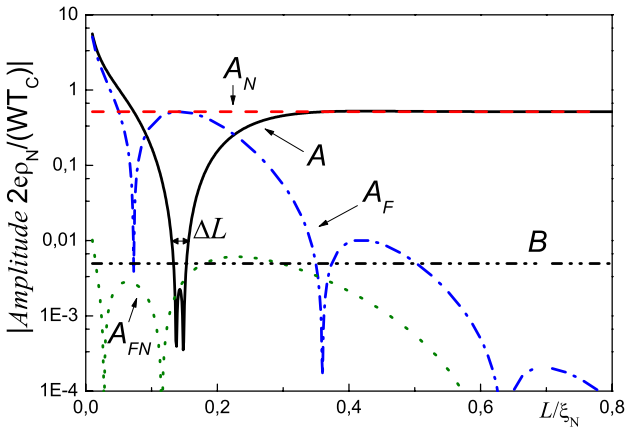

Figure 3. Analytically derived amplitudes A and B in the CPR of the ramp S–NF–S structure ($d_N = 0.1\xi_N$, $d_F = 0.65\xi_N$) and their components A_N, A_F and A_{FN} versus electrode spacing L at $T = 0.7T_C$. Also the enhanced interval of the φ-state, ΔL, is marked.

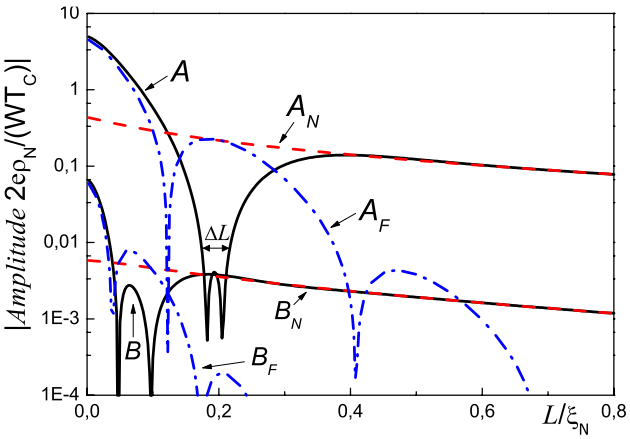

Figure 4. Numerically calculated CPR amplitudes A and B in the CPR of the ramp S–NF–S structure ($d_N = 0.1\xi_N$, $d_F = 1.06\xi_N$) and their components A_N, A_F, B_N and B_F versus electrode spacing L at $T = 0.7T_C$. In correspondence with figure 3 parameters are chosen to form an enhanced φ-state interval marked by 'ΔL'.

In the derivation of this inequality we have used the fact that for the range of distances between the electrodes $\pi/4 < \kappa L < 5\pi/4$ the factor $\exp(-\frac{\kappa L}{2})\sin(\frac{\kappa L}{2})$ in (29) is of the order of unity. It follows from (30) that for a fixed value of γ_{BFN} the domain of φ-junction existence extends with an increase of thickness of normal films d_N and this domain disappears if d_N becomes smaller than the critical value, d_{NC},

$$d_{NC} = \frac{\rho_N \xi_N}{h\rho_F \gamma_{BFN}} \left(\frac{\xi_F}{\xi_N \gamma_{BFN} h^{1/2}} + \frac{\gamma_{BN}}{\gamma_{BF}} \right). \qquad (31)$$

The existence of the critical thickness d_{NC} follows from the fact that the amplitude B in I_N is proportional to d_N, while in the I_{FN} term the parameter B is independent of d_N. The sign of $I_{FN1}(\varphi)$ is positive for $\pi/4 < \kappa L < 3\pi/4$ and negative for $3\pi/4 < \kappa L < 5\pi/4$, thus providing an advantage for a φ-junction realization for the lengths which belong to the second interval.

Figure 3 illustrates our analysis. The solid line in figure 3 is the modulus of the amplitude of the first harmonic in the CPR as a function of distance L between S electrodes. It is the result of the summation of the two contributions following from equations (17) (dash-dotted line) and (12) (dashed line). The dash–dot-dotted line in figure 3 is the amplitude of the second harmonic of the CPR following from (12). The dotted line is $I_{FN}(L)$ calculated from (18), (B.15)–(B.17). All calculations have been done for a set of parameters $d_N = 0.1\xi_N$, $d_F = 0.65\xi_N$, $\gamma_{BN} = 0.1$, $\gamma_{BF} = 1$, $\gamma_{BNF} = 10$, $\xi_F = 0.1\xi_N$, $\rho_N = \rho_F$, $T = 0.7T_C$, $H = 10T_C$. These parameters are close to those in the real experimental situation. All the amplitudes were normalized by the factor $(2e\rho_N/(WT_C))^{-1}$. It is evident that there is an interval of L for which the currents in the N-layer and F-layer flow in opposite directions. As a result of the addition of these currents the points of the 0 to π transitions start to be closer to each other. It is seen that in the entire region between these points, the inequality (2) is fulfilled. This is exactly the L-interval, inside which a φ-junction can be realized. It is also seen that contribution of the I_{FN} part into the full current is small and in accordance with our analysis does not play a noticeable role.

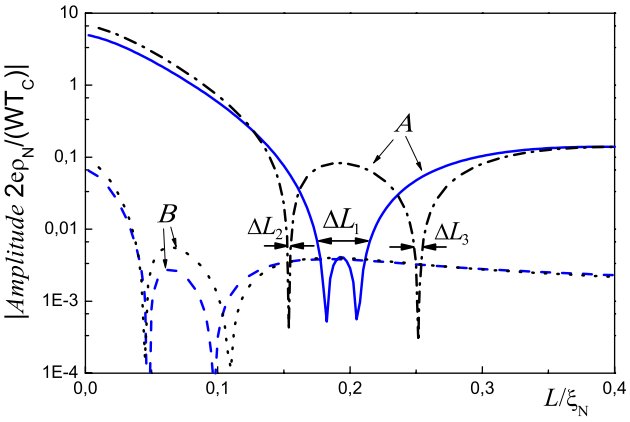

Figure 5. Numerically calculated CPR amplitudes A and B versus electrode spacing L for S–FN–S structures with $d_F = 1.06\xi_N$ (solid and dashed lines respectively) and $d_F = 1.4\xi_N$ (dash-dotted and dotted lines). It is clear that the enhanced φ-interval ΔL_1 formed in the first case is much larger than the pair of ordinary φ-intervals ΔL_2 and ΔL_3 in the second case.

The boundary problem (4)–(9*b*) has been solved numerically for the same set of junction parameters except d_F. The results of calculations for $d_F = 1.06\xi_N$ and $d_F = 1.4\xi_N$ are shown in figures 4 and 5. The solid lines in figure 4 are the modulus of the amplitudes of the first, A, and the second, B, harmonic of the CPR as a function of distance L between S electrodes. The dashed and dash-dotted lines demonstrate the contributions to these amplitudes from the currents flowing in the N and F films, respectively. All the amplitudes were normalized by the same factor $(2e\rho_N/(WT_C))^{-1}$. It is seen that the main difference between the analytical solutions presented in figure 3 and the curves calculated numerically are located in the region of small L. It is also seen that the amplitudes of the first and second harmonics of the part of the current flowing in the N film slightly decay with an increase of L. The points of the 0 to π transition of the first harmonic amplitude of the part of the current flowing in the F-layer is

slightly shifted to the right, towards larger L. It is also seen that the amplitude of the second harmonic, B_F, in the interval of interest in the vicinity of $L \approx 0.2\xi_N$ is negligibly small compared to the magnitude of B_N. As a result, the shape of the $A(L)$ curves in figures 3 and 4 is nearly the same, with a slightly larger interval of φ-junction existence for the curve calculated numerically.

Figure 5 demonstrates the same $A(L)$ and $B(L)$ dependences as in figure 4 (solid and dashed lines) together with $A(L)$ and $B(L)$ curves calculated for $d_F = 1.4\xi_N$ (dash-dotted and dotted lines). It is clearly seen that for larger d_F we get out of the interval (26) and instead of a relatively large zone ΔL_1 may have a φ-junction in two very narrow intervals ΔL_2 and ΔL_3 located in the vicinity of the 0 to π transitions of the first harmonic amplitude A.

5. Ramp-type overlap (RTO) junctions

The conditions for the existence of the φ-junction, (25) and (26) can be improved by slight modifications of the contact geometry, namely, by using a combination of ramp and overlap configurations, as is shown in figure 1(b). Figure 6 demonstrates the numerically calculated spatial distribution of the supercurrent in the RTO φ-junction at the Josephson phase $\varphi = \pi/2$. The current density is presented by the darkness and the arrows give flow directions. The relative smallness of the first harmonic amplitude is provided by opposite currents in the N and F films. The main feature of the ramp-overlap geometry is seen to be a specific current distribution in the normal layer leading to another CPR shape with dependence on thickness d_N. Furthermore, the current I_N should saturate as a function of d_N, since normal film regions located at distances larger than ξ_N from the SN interface are practically excluded from the process of supercurrent transfer due to the exponential decay of proximity-induced superconducting correlations [74]. The specific geometry of the RTO structures makes theoretical analysis of the processes more complex than in ramp contact. Nevertheless, it is possible to find analytical expressions for the supercurrent in these structures and to show that the range of parameters providing the existence of the φ-state is broader than in the ramp-type configuration.

To prove this statement, we consider the RTO structure in the most practical case of a thin N film

$$d_N \ll \xi_N \tag{32}$$

and sufficiently large γ_{BFN} providing negligibly small suppression of superconductivity in the N film due to proximity to the F-layer. We will assume additionally that the electrode spacing L is also small

$$L \ll \xi_N, \tag{33}$$

in order to have a non-sinusoidal CPR. Under these conditions we can at the first step consider the Josephson effect in the overlap SN–N–NS structure. Then, at the second step we will use the obtained solutions to calculate the supercurrent flowing across the F part of the RTO structure. The details of

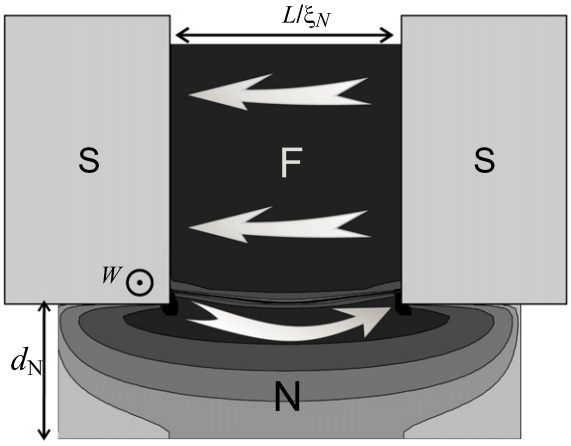

Figure 6. Current distribution along the RTO-type SN–FN–NS structure at $L = 0.63\xi_N$, $d_N = \xi_N$, $d_F = 2\xi_N$ and $T = 0.7T_C$. The intensity of gray color shows the current density in the direction indicated by arrows.

the calculations are summarized in appendices C and D. They give that the supercurrent

$$I_S(\varphi) = I_N(\varphi) + I_F(\varphi) + I_{FN}(\varphi) \tag{34}$$

consists of three components. The expression for the part of the current flowing across the N film has the form

$$\frac{2eI_N(\varphi)}{\pi TWd_N} = \frac{2}{\rho_N\xi_N\sqrt{\gamma_{BM}}} \times \sum_{\omega=-\infty}^{\infty} \frac{r^2\delta^2 \sin\varphi\sqrt{(\Omega\gamma_{BM} + G_S)}}{\sqrt{2\Omega\mu^2(\sqrt{\Omega^2 + r^2\delta^2} + \mu)}}, \tag{35}$$

where $r = G_S/(\Omega\gamma_{BM} + G_S)$, $\gamma_{BM} = \gamma_{BN}d_N/\xi_N$ and $\mu = \sqrt{\Omega^2 + r^2\delta^2\cos^2(\varphi/2)}$, $\delta = \Delta/\pi T_C$.

The $I_F(\varphi)$ term in (34) is the current through the one-dimensional double-barrier SFS structure defined by equation (17), while $I_{FN}(\varphi)$ is the FN interface term shown in appendix D. We provide sufficient smallness and neglect it in the following estimations.

As we discussed above, the larger the relative amplitude of the second harmonic (or the lower the temperature of a junction compare to T_C), the better the conditions for the implementation of a φ-contact. In the limit $T \ll T_C$, we can transform from summation to integration over ω in (35) and calculate numerically the dependence of amplitudes A and B

$$A_N = \frac{2W\Delta}{e\rho_N\gamma_{BN}}\Upsilon_A, \tag{36}$$

$$B_N = \frac{2W\Delta}{e\rho_N\gamma_{BN}}\Upsilon_B \tag{37}$$

on the suppression parameter γ_{BM}. The calculated dependences of functions $\Upsilon_A(\gamma_{BM})$ and $\Upsilon_B(\gamma_{BM})$ are presented in figure 7. It is seen that both Υ_A and $|\Upsilon_B|$ increase with increasing γ_{BM} and saturate at $\gamma_{BM} \approx 1$. The inset in figure 7 shows the ratio of the harmonics $|\Upsilon_B/\Upsilon_A|$ as a function of γ_{BM}. It achieves a maximum at $\gamma_{BM} \approx 0.64$ and thus determines the optimal values of normalized amplitudes of the

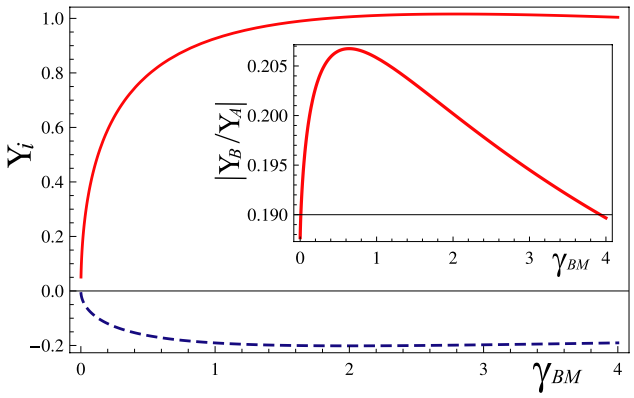

Figure 7. Coefficients Υ_A (solid line) and Υ_B (dashed line) in equations (36)–(37) as a function of suppression parameter γ_{BM}. Inset shows the ratio $|\Upsilon_B/\Upsilon_A|$ versus γ_{BM}.

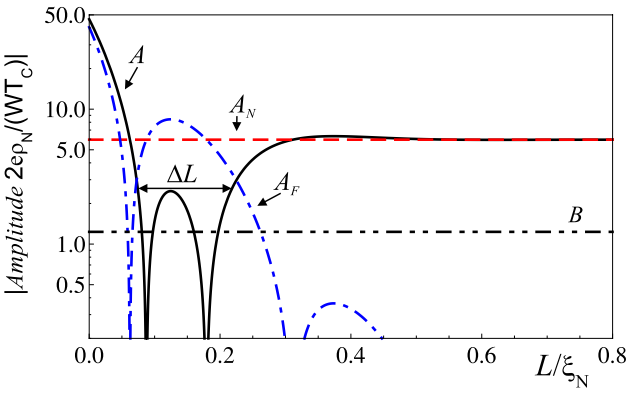

Figure 8. The amplitudes of the CPR harmonics A, A_N, A_F and B versus electrode spacing L for the RTO structure at $T \ll T_C$, $\gamma_{BM} = 0.64$ and $\varepsilon = 0.123$. The mark 'ΔL' shows the enhanced φ-state interval.

first, $\Upsilon_A \approx 0.844$, and the second, $\Upsilon_B \approx -0.175$, harmonics of the current flowing in the N-layer. It is seen from the inset in figure 7, that the ratio $|\Upsilon_B/\Upsilon_A|$ is a slowly decreasing function of γ_{BM}. Therefore, the estimates given below for $\gamma_{BM} = 0.64$ are applicable in a wide parameter range $0.5 \leq \gamma_{BM} \leq 10$.

Taking into account these values, we can write down the conditions for φ-state existence similar to (23)

$$\left|\Upsilon_A + \frac{1}{\varepsilon}\Psi(L)\right| \leq 2|\Upsilon_B|, \qquad \varepsilon = \frac{\sqrt{h}\gamma_{BF}^2}{\gamma_{BN}}\frac{\xi_F\rho_F}{d_F\rho_N}, \quad (38)$$
$$\Psi(L) = \exp(-\kappa L)\cos\left(\kappa L + \frac{\pi}{4}\right),$$

with a slightly modified dimensionless parameter ε. The wide region of the φ-state still exists if ε is within the interval

$$0.123 \lesssim \varepsilon \lesssim 0.298 \quad (39)$$

for κL that satisfies the conditions (38). As follows from (38), the interval of the κL product reaches its maximum length

$$0.94 \lesssim \kappa L \lesssim 2.72, \quad (40)$$

at $\varepsilon = 0.123$. It is seen that these intervals are slightly larger than those given by (25) for the ramp-type geometry.

Figure 8 shows the interval of φ-state existence, ΔL, in the ideal case of $T \ll T_C$, $\gamma_{BM} = 0.64$ and $\varepsilon = 0.123$. The corresponding set of parameters $d_N = 0.64\xi_N$, $d_F = 1.45\xi_N$, $\gamma_{BN} = 1$, $\gamma_{BF} = 1$, $\xi_F = 0.1\xi_N$, $\rho_N = \rho_F$, $H = 10T_C$ was substituted in (17) and (35). The solid line is the modulus of the first harmonic amplitude, A, its normal, A_N, and ferromagnetic, A_F, parts, presented by dashed and dash-dotted lines respectively. Finally, the second harmonic amplitude is shown as a dash–dot-dotted line. It is clear that $|A|$ is relatively small in the wide region ΔL and reaches the value of $|2B|$ only at the local maximum. The increased width of ΔL (see equations (25) and (40)) is provided by the geometric attributes of the RTO-type structure.

Let us illustrate the range of nontrivial ground state phase φ_g existence in the structure described in figure 8. The total supercurrent I_S is shown on figure 9 as a function of Josephson phase φ and electrode spacing L. It means that each L-section of this 3D graph is the CPR. Solid lines mark the ground state phases at each L. In the range of small and large spacing L, the ground state phase is located at $\varphi_g = 0$. However, in the ΔL-interval the CPR becomes significantly non-sinusoidal and requires the ground state phase φ_g to split and go to π from both sides; then the π-state is realized at $\kappa L = \pi/2$. Clearly, for $\varepsilon \gtrsim 0.123$ the value $\varphi_g = \pi$ cannot be reached (see figure 9(a)), while in the case of $\varepsilon \lesssim 0.123$ the prolonged π-state region is formed (see figure 9(c)).

6. Discussion

We have shown that the stable φ-state can be realized in S–NF–S structures with longitudinally oriented NF-bilayers (though the φ-state cannot be achieved in conventional SNS and SFS structures). We have discussed the conditions for realization of the φ-state in ramp-type S–NF–S and RTO-type SN–FN–NS geometries.

Let us discuss the most favorable conditions for experimental realization of the φ-junction. We suggest using copper as a normal film ($\xi_N \approx 100$ nm and $\rho = 5 \times 10^{-8}$ Ω m) and a strongly diluted ferromagnet such as FePd or CuNi alloy ($\xi_F \approx 10$ nm, $H \approx 10T_C$) as the F-layer. We chose Nb ($T_C \approx 9$ K) as a superconducting electrode material since it is commonly used in superconducting circuit applications. We also propose to use a sufficiently thick normal layer, above the saturation threshold, when the N-layer thickness has almost no effect. After substitution of the relevant values into (39) and (40) we arrived at fairly broad geometrical margins, within which there is a possibility for implementation of φ-junctions

$$d_N \gtrsim 50 \text{ nm}, \qquad 60 \text{ nm} \lesssim d_F \lesssim 150 \text{ nm}, \qquad 7 \text{ nm} \lesssim L \lesssim 22 \text{ nm}. \quad (41)$$

Finally, the last out-of-plane geometrical scale is set as $W = 140$ nm. This value maximizes the current and conserves the scale of the structure in a range of 100 nm. The magnitude of critical supercurrent in the φ-state is determined by the second harmonic amplitude B

$$I_C \sim B_N = \frac{2W\Delta}{e\rho_N\gamma_{BN}}\Upsilon_B \approx 1 \text{ mA}. \quad (42)$$

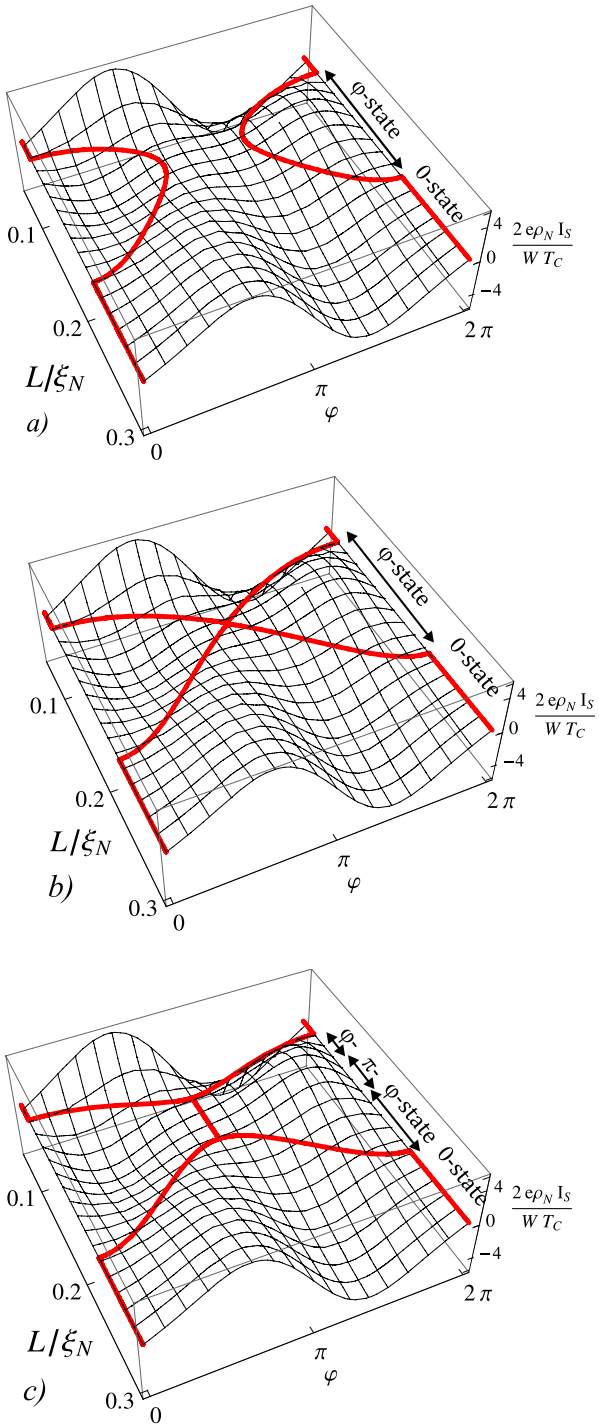

Figure 9. The full current I_S versus Josephson phase φ and electrode spacing L for the RTO structure at $T \ll T_C$, $\gamma_{BM} = 0.64$ and at different F-layer thickness parameters (a) $\varepsilon = 0.137$, (b) $\varepsilon = 0.123$ and (c) $\varepsilon = 0.111$. The lines mark the ground state phase φ_g.

The spreads of geometrical scales as well as the magnitude of critical current are large enough to be realized experimentally.

By creating the φ-state in a Josephson junction one can fix a certain value of ground state phase φ_g. The temperature variation slightly shifts the interval of relevant 0 to π transition and permits one to tune the desired ground state phase. Furthermore, the sensitivity of the ground state to an electron distribution function permits φ-junctions to be applied as small-scale self-biasing one-photon detectors. Moreover, a quantum double-well potential is formed at the point of ground state splitting, providing the necessary condition for quantum bits and quantum detectors. To summarize, Josephson φ-junctions can be realized using up-to-date technology and may become important basic elements in superconducting electronics.

Acknowledgments

We gratefully acknowledge V V Ryazanov helpful discussions. This work was supported by the Russian Foundation for Basic Research (Grants 12-02-90010-Bel-a, 11-02-12065-ofi-m), Russian Ministry of Education and Science (Agreement N8746), Dynasty Foundation and Dutch FOM.

Appendix A. Ramp-type junctions. Limit of small L

In the limit of small spacing between S electrodes

$$L \ll \min\{\xi_F, \xi_N\} \tag{A.1}$$

we can neglect non-gradient terms in (4)

$$\frac{\partial}{\partial x}\left(G_{F,N}^2 \frac{\partial}{\partial x} R_{F,N}\right) + \frac{\partial}{\partial z}\left(G_{F,N}^2 \frac{\partial}{\partial z} R_{F,N}\right) = 0, \tag{A.2}$$

$$\frac{\partial}{\partial x}\left(G_{F,N}^2 \frac{\partial}{\partial x} U_{F,N}\right) + \frac{\partial}{\partial z}\left(G_{F,N}^2 \frac{\partial}{\partial z} U_{F,N}\right) = 0, \tag{A.3}$$

and introduce four functions

$$\Phi_F = R_F + iU_F, \qquad \Phi_N = R_N + iU_N, \tag{A.4}$$

where, i is the imaginary unit, R_F and R_N are even functions of coordinate x, and U_F and U_N are odd in x. Due to the symmetry at $x = 0$

$$\frac{\partial R_{F,N}}{\partial x} = 0, \qquad U_{F,N} = 0 \tag{A.5}$$

for any coordinate z, and it is convenient to rewrite boundary conditions (9*a*) and (9*b*) at $x = L/2$ in the form

$$\gamma_{BN}\xi_N \frac{\partial R_N}{\partial x} = \frac{G_S}{G_N}(\Delta \cos(\varphi/2) - R_N), \tag{A.6}$$

$$\gamma_{BF}\xi_F \frac{\partial R_F}{\partial x} = \frac{G_S}{G_F}\left(\frac{\tilde{\omega}}{\omega}\Delta \cos(\varphi/2) - R_F\right), \tag{A.7}$$

$$\gamma_{BN}\xi_N \frac{\partial U_N}{\partial x} = \frac{G_S}{G_N}(\Delta \sin(\varphi/2) - U_N), \tag{A.8}$$

$$\gamma_{BF}\xi_F \frac{\partial U_F}{\partial x} = \frac{G_S}{G_F}\left(\frac{\tilde{\omega}}{\omega}\Delta \sin(\varphi/2) - U_F\right). \tag{A.9}$$

At the NF interface the boundary conditions transform to

$$\gamma_{BFN}\xi_F \frac{\partial R_F}{\partial z} = -\frac{G_N}{G_F}\left(R_F - \frac{\tilde{\omega}}{\omega} R_N\right), \tag{A.10}$$

$$\gamma_{BNF}\xi_N \frac{\partial R_N}{\partial z} = \frac{G_F}{G_N}\left(R_N - \frac{\omega}{\tilde{\omega}} R_F\right), \tag{A.11}$$

$$\gamma_{\mathrm{BFN}}\xi_{\mathrm{F}}\frac{\partial U_{\mathrm{F}}}{\partial z} = -\frac{G_{\mathrm{N}}}{G_{\mathrm{F}}}\left(U_{\mathrm{F}} - \frac{\tilde{\omega}}{\omega}U_{\mathrm{N}}\right), \qquad \text{(A.12)}$$

$$\gamma_{\mathrm{BNF}}\xi_{\mathrm{N}}\frac{\partial U_{\mathrm{N}}}{\partial z} = \frac{G_{\mathrm{F}}}{G_{\mathrm{N}}}\left(U_{\mathrm{N}} - \frac{\omega}{\tilde{\omega}}U_{\mathrm{F}}\right). \qquad \text{(A.13)}$$

From (A.5) and (A.6)–(A.9) it follows that for γ_{BF} and γ_{BN} within the interval

$$\frac{L}{\xi_{\mathrm{N}}} \ll \gamma_{\mathrm{BN}} \ll \frac{\xi_{\mathrm{N}}}{L}, \qquad \frac{L}{\xi_1} \ll \gamma_{\mathrm{BF}} \ll \frac{\xi_1}{L}, \qquad \text{(A.14)}$$

we can neglect $U_{\mathrm{N,F}}$ on the left-hand side of (A.8) and (A.9). Moreover, in this approximation, for any point inside the weak link region $R_{\mathrm{F,N}} \gg U_{\mathrm{F,N}}$ and the boundary problem (A.2)–(A.13) for functions R_{F} and R_{N} can be solved, resulting in

$$R_{\mathrm{N}} = \Delta\cos(\varphi/2), \qquad R_{\mathrm{F}} = \frac{\tilde{\omega}}{\omega}\Delta\cos(\varphi/2) \qquad \text{(A.15)}$$

and

$$G_{\mathrm{N}} = G_{\mathrm{F}} = \frac{\omega}{\sqrt{\omega^2 + \Delta^2\cos^2(\varphi/2)}}. \qquad \text{(A.16)}$$

Therefore under conditions (A.14) both G_{N} and G_{F} are functions independent of coordinate x, z and the equations for $U_{\mathrm{F,N}}$ transform to Laplace equations, which have the solutions

$$U_{\mathrm{N}} = \frac{\Delta\sin(\varphi/2)}{\gamma_{\mathrm{BN}}}\frac{G_{\mathrm{S}}}{G_{\mathrm{N}}}\frac{x}{\xi_{\mathrm{N}}} + \sum_{n=1}^{\infty} a_n \sin\frac{\pi(2n+1)x}{L} \times \cosh\frac{\pi(2n+1)(z - d_{\mathrm{N}} - d_{\mathrm{F}})}{L}, \qquad \text{(A.17)}$$

$$U_{\mathrm{F}} = \frac{\Delta\sin(\varphi/2)}{\gamma_{\mathrm{BF}}}\frac{\tilde{\omega}}{\omega}\frac{G_{\mathrm{S}}}{G_{\mathrm{F}}}\frac{x}{\xi_{\mathrm{F}}} + \frac{\tilde{\omega}}{\omega}\sum_{n=1}^{\infty} b_n \sin\frac{(2n+1)\pi x}{L}\cosh\frac{\pi(2n+1)z}{L}. \qquad \text{(A.18)}$$

They automatically satisfy the boundary conditions at $z = 0$ and $d_{\mathrm{N}}+d_{\mathrm{F}}$, as well as at $x = 0$ and $L/2$. To find the integration constants a_n and b_n we have to substitute (A.17) and (A.18) into (A.12) and (A.13) and get

$$a_n = -\frac{\Delta\sin(\varphi/2)G_{\mathrm{S}}\Theta\gamma_{\mathrm{BFN}}\xi_{\mathrm{F}}t_n}{G_{\mathrm{N}}\beta\cosh\frac{\pi(2n+1)d_{\mathrm{N}}}{L}}, \quad t_n = \tanh\frac{\pi(2n+1)d_{\mathrm{N}}}{L}, \quad b_n = \frac{\Delta\sin(\varphi/2)G_{\mathrm{S}}\Theta\gamma_{\mathrm{BNF}}\xi_{\mathrm{N}}t_f}{G_{\mathrm{N}}\beta\cosh\frac{\pi(2n+1)d_{\mathrm{F}}}{L}}, \quad t_f = \tanh\frac{\pi(2n+1)d_{\mathrm{F}}}{L}, \qquad \text{(A.19)}$$

where

$$\beta = \left(\gamma_{\mathrm{BNF}}\xi_{\mathrm{N}}\frac{\pi(2n+1)}{L}t_n + 1\right)\gamma_{\mathrm{BFN}}\xi_{\mathrm{F}}t_f + \gamma_{\mathrm{BNF}}\xi_{\mathrm{N}}t_n,$$

and

$$\Theta = \left(\frac{1}{\gamma_{\mathrm{BN}}\xi_{\mathrm{N}}} - \frac{1}{\gamma_{\mathrm{BF}}\xi_{\mathrm{F}}}\right)\frac{4L}{\pi^2}\frac{(-1)^n}{(2n+1)^2}.$$

Substitution of (A.17) and (A.18) into the expression for the supercurrent (5) gives that contributions to the supercurrent across the junction proportional to a_n and b_n cancel each other and $I_{\mathrm{S}}(\varphi)$ equals the sum

$$I_{\mathrm{S}}(\varphi) = I_{\mathrm{N}}(\varphi) + I_{\mathrm{F}}(\varphi), \quad \frac{2eI_{\mathrm{N}}(\varphi)}{\pi TWd_{\mathrm{N}}} = \frac{1}{\gamma_{\mathrm{BN}}\xi_{\mathrm{N}}\rho_{\mathrm{N}}}\sum_{\omega=-\infty}^{\infty}\frac{\Delta^2 G_{\mathrm{N}}G_{\mathrm{S}}\sin(\varphi)}{\omega^2}, \qquad \text{(A.20)}$$

$$\frac{2eI_{\mathrm{F}}(\varphi)}{\pi TWd_{\mathrm{F}}} = \frac{1}{\gamma_{\mathrm{BF}}\xi_{\mathrm{F}}\rho_{\mathrm{F}}}\sum_{\omega=-\infty}^{\infty}\frac{\Delta^2 G_{\mathrm{F}}G_{\mathrm{S}}\sin(\varphi)}{\omega^2} \qquad \text{(A.21)}$$

of the currents, $I_{\mathrm{N}}(\varphi)$ and $I_{\mathrm{F}}(\varphi)$, flowing independently across the F and N parts of the weak link.

Appendix B. Ramp-type junctions. Limit of intermediate *L*

For intermediate values of spacing between the S electrodes

$$\xi_1 \ll L \ll \xi_{\mathrm{N}} \qquad \text{(B.1)}$$

and suppression parameters at SN and SF interfaces belonging to the interval (3) the boundary problem (4)–(9*b*) can be also solved analytically for sufficiently large suppression parameter γ_{BFN}. Under these restrictions, in the first approximation we can neglect the suppression of superconductivity in the N film due to proximity to the F-layer and use expressions (A.15) and (A.18) with $a_n = 0$ as the solution in the N part of the weak link.

To find R_{F} and U_{F} we have to solve the linear equations

$$\xi_{\mathrm{F}}^2\frac{\partial^2}{\partial x^2}R_{\mathrm{F}} + \xi_{\mathrm{F}}^2\frac{\partial^2}{\partial z^2}R_{\mathrm{F}} - \tilde{\Omega}R_{\mathrm{F}} = 0, \qquad \text{(B.2)}$$

$$\xi_{\mathrm{F}}^2\frac{\partial^2}{\partial x^2}U_{\mathrm{F}} + \xi_{\mathrm{F}}^2\frac{\partial^2}{\partial z^2}U_{\mathrm{F}} - \tilde{\Omega}U_{\mathrm{F}} = 0, \qquad \text{(B.3)}$$

with the boundary conditions

$$\gamma_{\mathrm{BF}}\xi_{\mathrm{F}}\frac{\partial R_{\mathrm{F}}}{\partial x} = G_{\mathrm{S}}\frac{\tilde{\Omega}}{\Omega}\Delta\cos(\varphi/2), \qquad \text{(B.4)}$$

$$\gamma_{\mathrm{BF}}\xi_{\mathrm{F}}\frac{\partial U_{\mathrm{F}}}{\partial x} = G_{\mathrm{S}}\frac{\tilde{\Omega}}{\Omega}\Delta\sin(\varphi/2), \qquad \text{(B.5)}$$

at $x = L/2$, $0 \le z \le d_{\mathrm{F}}$ and

$$\gamma_{\mathrm{BFN}}\xi_{\mathrm{F}}\frac{\partial R_{\mathrm{F}}}{\partial z} = \frac{\tilde{\Omega}}{\Omega}G_{\mathrm{N}}R_{\mathrm{N}}, \qquad \text{(B.6)}$$

$$\gamma_{\mathrm{BFN}}\xi_{\mathrm{F}}\frac{\partial U_{\mathrm{F}}}{\partial z} = \frac{\tilde{\Omega}}{\Omega}G_{\mathrm{N}}U_{\mathrm{N}}, \qquad \text{(B.7)}$$

at $z = d_{\mathrm{F}}$, $0 \le x \le L/2$; ($\Omega = \omega/\pi T_{\mathrm{C}}$, $\tilde{\Omega} = \tilde{\omega}\mathrm{sgn}(\omega)/\pi T_{\mathrm{C}}$). The boundary problem (B.2)–(B.7) must be closed by the conditions (7) and (A.5) at the free interface of the F film and at the line of junction symmetry, respectively.

The spatial distribution for the part of $\Phi_{\mathrm{F}}(x, z)$ that is even in coordinate x can be found in the form of the superposition of superconducting correlations induced into the F film from

superconductors and from the N part of the weak link

$$R_{\mathrm{F}} = \frac{\sqrt{\tilde{\Omega}}G_{\mathrm{S}}\Delta\cos(\varphi/2)}{\Omega\gamma_{\mathrm{BF}}}\frac{\cosh(\sqrt{\tilde{\Omega}}\frac{x}{\xi_{\mathrm{F}}})}{\sinh(\sqrt{\tilde{\Omega}}\frac{L}{2\xi_{\mathrm{F}}})} + \frac{\sqrt{\tilde{\Omega}}G_{\mathrm{N}}\Delta\cos(\varphi/2)}{\Omega\gamma_{\mathrm{BFN}}}\frac{\cosh(\sqrt{\tilde{\Omega}}\frac{z}{\xi_{\mathrm{F}}})}{\sinh(\sqrt{\tilde{\Omega}}\frac{d_{\mathrm{F}}}{\xi_{\mathrm{F}}})}. \tag{B.8}$$

The solution for the odd part of $\Phi_{\mathrm{F}}(x, z)$ consist of three terms

$$U_{\mathrm{F}} = \frac{\sqrt{\tilde{\Omega}}G_{\mathrm{S}}\Delta\sin(\varphi/2)}{\Omega\gamma_{\mathrm{BN}}\gamma_{\mathrm{BFN}}}\frac{x\cosh(\sqrt{\tilde{\Omega}}\frac{z}{\xi_{\mathrm{F}}})}{\xi_{\mathrm{N}}\sinh(\sqrt{\tilde{\Omega}}\frac{d_{\mathrm{F}}}{\xi_{\mathrm{F}}})} - \frac{\tilde{\Omega}^{3/2}G_{\mathrm{S}}\Delta\sin(\varphi/2)\xi_{\mathrm{F}}^2}{\Omega\gamma_{\mathrm{BN}}\xi_{\mathrm{N}}\gamma_{\mathrm{BFN}}d_{\mathrm{F}}} \times \sum_{n=-\infty}^{\infty}\frac{(-1)^n\cos(\frac{\pi n z}{d_{\mathrm{F}}})\sinh(\kappa_n\frac{x}{\xi_{\mathrm{F}}})}{\kappa_n^3\cosh(\kappa_n\frac{L}{2\xi_{\mathrm{F}}})} + \frac{\sqrt{\tilde{\Omega}}G_{\mathrm{S}}\Delta\sin(\varphi/2)}{\Omega\gamma_{\mathrm{BF}}}\frac{\sinh(\sqrt{\tilde{\Omega}}\frac{x}{\xi_{\mathrm{F}}})}{\cosh(\sqrt{\tilde{\Omega}}\frac{L}{2\xi_{\mathrm{F}}})}, \tag{B.9}$$

where $\kappa_n^2 = \tilde{\Omega} + (\pi n\xi_{\mathrm{F}}/d_{\mathrm{F}})^2$. The first two give the part of U_{F} induced from the N film, while the last has the well-known form for SFS junctions [2–4].

From (B.8) and (B.9) it follows that $R^*_{-\omega,\mathrm{F}} = R_{\omega,\mathrm{F}}$ and $U^*_{-\omega,\mathrm{F}} = U_{\omega,\mathrm{F}}$. Substitution of (B.8) and (B.9) into the expression for the supercurrent (5) gives that the $I_{\mathrm{S}}(\varphi)$ dependence consists of three terms

$$I_{\mathrm{S}}(\varphi) = I_{\mathrm{N}}(\varphi) + I_{\mathrm{F}}(\varphi) + I_{\mathrm{FN}}(\varphi). \tag{B.10}$$

The first is the supercurrent across the N-layer. In the considered approximation it coincides with the expression given by (A.20). The second term in (B.10) is the supercurrent across the SFS double-barrier structure in the limit of small transparencies of SF interfaces [72, 73]

$$\frac{2eI_{\mathrm{F}}(\varphi)}{\pi TWd_{\mathrm{F}}} = \frac{\Delta^2\sin(\varphi)}{\gamma_{\mathrm{BF}}^2\xi_{\mathrm{F}}\rho_{\mathrm{F}}}\sum_{\omega=-\infty}^{\infty}\frac{G_{\mathrm{S}}^2}{\omega^2\sqrt{\tilde{\Omega}}\sinh(2q_L)} \tag{B.11}$$

and the last consists of two terms, $I_{\mathrm{FN}}(\varphi) = I_1(\varphi) + I_2(\varphi)$ having different φ-dependence

$$\frac{2eI_1(\varphi)}{\pi TWd_{\mathrm{F}}} = \frac{\Delta^2\sin(\varphi)}{\rho_{\mathrm{F}}d_{\mathrm{F}}}\frac{\xi_{\mathrm{F}}}{\gamma_{\mathrm{BF}}\gamma_{\mathrm{BFN}}\gamma_{\mathrm{BN}}\xi_{\mathrm{N}}}\sum_{\omega=-\infty}^{\infty}\frac{G_{\mathrm{S}}^2}{\tilde{\Omega}^2\omega^2}\Psi_1, \qquad \Psi_1 = \frac{\sqrt{\tilde{\Omega}}}{\sinh(q_L)} - \frac{2\tilde{\Omega}}{\sinh(2q_L)}, \tag{B.12}$$

$$\frac{2eI_2(\varphi)}{\pi TWd_{\mathrm{F}}} = \frac{\Delta^2\sin(\varphi)}{\gamma_{\mathrm{BFN}}\rho_{\mathrm{F}}d_{\mathrm{F}}}\sum_{\omega=-\infty}^{\infty}\frac{G_{\mathrm{N}}G_{\mathrm{S}}}{\omega^2\tilde{\Omega}^2} \times\left(\frac{1}{\gamma_{\mathrm{BN}}\gamma_{\mathrm{BFN}}\xi_{\mathrm{N}}}\Psi_2 + \frac{\tilde{\Omega}}{\gamma_{\mathrm{BF}}\cosh q_L}\right), \qquad \Psi_2 = \frac{d_{\mathrm{F}}\tilde{\Omega}(2q_d + \sinh(2q_d))}{4q_d\sinh^2(q_d)} - \frac{\tilde{\Omega}\xi_{\mathrm{F}}}{q_d\cosh(q_L)} - \sum_{n=1}^{\infty}\frac{2\tilde{\Omega}^3\xi_{\mathrm{F}}}{q_d\kappa_n^4\cosh(\frac{L\kappa_n}{2\xi_{\mathrm{F}}})}, \tag{B.13}$$

where $q_d = d_{\mathrm{F}}\sqrt{\tilde{\Omega}}/\xi_{\mathrm{F}}$, $q_L = L\sqrt{\tilde{\Omega}}/2\xi_{\mathrm{F}}$. In the real experimental situation

$$\xi_{\mathrm{F}} \ll \xi_{\mathrm{N}}, \qquad d_{\mathrm{F}} \gg \xi_{\mathrm{F}}. \tag{B.14}$$

Under the conditions (B.14) some terms of $I_{\mathrm{FN}}(\varphi)$ can be neglected. The remaining expressions of its parts $I_{\mathrm{FN1}}(\varphi)$ - $I_{\mathrm{FN3}}(\varphi)$ simplify to

$$\frac{2eI_{\mathrm{FN1}}(\varphi)}{\pi TWd_{\mathrm{F}}} = \frac{\Delta^2\sin(\varphi)}{\gamma_{\mathrm{BF}}\gamma_{\mathrm{BFN}}\gamma_{\mathrm{BN}}\rho_{\mathrm{F}}d_{\mathrm{F}}} \times\frac{\xi_{\mathrm{F}}}{\xi_{\mathrm{N}}}\sum_{\omega=-\infty}^{\infty}\frac{G_{\mathrm{S}}^2}{\omega^2\tilde{\Omega}^2}\frac{\sqrt{\tilde{\Omega}}}{\sinh q_L}, \tag{B.15}$$

$$\frac{2eI_{\mathrm{FN2}}(\varphi)}{\pi TWd_{\mathrm{F}}} = \frac{\Delta^2\sin(\varphi)}{2\gamma_{\mathrm{BN}}\gamma_{\mathrm{BFN}}^2\rho_{\mathrm{F}}d_{\mathrm{F}}}\sum_{\omega=-\infty}^{\infty}\frac{G_{\mathrm{N}}G_{\mathrm{S}}}{\omega^2\tilde{\Omega}^{3/2}}\frac{\xi_{\mathrm{F}}}{\xi_{\mathrm{N}}}, \tag{B.16}$$

$$\frac{2eI_{\mathrm{FN3}}(\varphi)}{\pi TWd_{\mathrm{F}}} = \frac{\Delta^2\sin(\varphi)}{\gamma_{\mathrm{BFN}}\gamma_{\mathrm{BF}}\rho_{\mathrm{F}}d_{\mathrm{F}}}\sum_{\omega=-\infty}^{\infty}\frac{G_{\mathrm{N}}G_{\mathrm{S}}}{\omega^2\tilde{\Omega}}\frac{1}{\cosh q_L}. \tag{B.17}$$

Appendix C. Overlap SN–N–NS junctions

To calculate critical current of SN–N–NS junctions we consider the most practical case of a thin N film

$$d_{\mathrm{N}} \ll \xi_{\mathrm{N}} \tag{C.1}$$

and sufficiently large γ_{BFN} providing the absence of suppression of superconductivity in the N film due to proximity to the F-layer. We will also assume that the electrode spacing L is also small

$$L \ll \xi_{\mathrm{N}}, \tag{C.2}$$

in order to have a non-sinusoidal CPR.

Condition (C.1) permits one to perform averaging of the Usadel equations in the z-direction in the N film, as was described in detail in [47], and reduce the problem to the solution of one-dimensional equations for $\Phi_{\mathrm{N}} = R_{\mathrm{N}} + \mathrm{i}U_{\mathrm{N}}$. The real part of Φ_{N} is the solution of the boundary problem

$$\frac{\xi_{\mathrm{N}}^2\gamma_{\mathrm{BM}}}{G_{\mathrm{N}}(\Omega\gamma_{\mathrm{BM}} + G_{\mathrm{S}})}\frac{\partial}{\partial x}\left(G_{\mathrm{N}}^2\frac{\partial R_{\mathrm{N}}}{\partial x}\right) - R_{\mathrm{N}} = -r\Delta\cos\frac{\varphi}{2}, \qquad \frac{L}{2} \le x \le \infty, \tag{C.3}$$

$$\frac{\xi_{\mathrm{N}}^2}{\Omega G_{\mathrm{N}}}\frac{\partial}{\partial x}\left(G_{\mathrm{N}}^2\frac{\partial R_{\mathrm{N}}}{\partial x}\right) = 0, \qquad 0 \le x \le \frac{L}{2}, \tag{C.4}$$

$$\frac{\partial R_{\mathrm{N}}}{\partial x} = 0, \qquad x = 0, \qquad x \to \infty, \tag{C.5}$$

where $r = G_{\mathrm{S}}/(\Omega\gamma_{\mathrm{BM}} + G_{\mathrm{S}})$, $\gamma_{\mathrm{BM}} = \gamma_{\mathrm{BN}}d_{\mathrm{N}}/\xi_{\mathrm{N}}$, $\delta = \Delta/\pi T_{\mathrm{C}}$.

From (C.4) and (C.5) it follows that at $0 \le x \le L/2$ functions R_{N} are constants independent of x, resulting in

$$\frac{\partial R_{\mathrm{N}}}{\partial x}\left(\frac{L}{2}\right) = 0. \tag{C.6}$$

The resultant boundary problem (C.3), (C.5) and (C.6) is also satisfied by constants independent of x, leading to

$$R_{\mathrm{N}} = r\Delta\cos(\varphi/2), \qquad 0 \le x < \infty. \tag{C.7}$$

Now, introducing new functions, θ

$$U_N = \mu \tan\theta, \qquad G_N = \frac{\Omega}{\mu}\cos\theta, \tag{C.8}$$

where $\mu = \sqrt{\Omega^2 + r^2\delta^2\cos^2(\varphi/2)}$, we get

$$\lambda^2 \frac{\partial^2}{\partial x^2}\theta - \sin(\theta - \phi) = 0, \qquad \frac{L}{2} \le x < \infty, \tag{C.9}$$

$$\frac{\xi_N^2}{\cos\theta}\frac{\partial^2}{\partial x^2}\theta = 0, \qquad 0 \le x \le \frac{L}{2}, \tag{C.10}$$

$$\theta(0) = 0, \qquad \frac{\partial\theta}{\partial x} = 0, \qquad x \to \infty, \tag{C.11}$$

where

$$\lambda = \xi_N \sqrt{\frac{\Omega\gamma_{BM}}{(\Omega\gamma_{BM} + G_S)\sqrt{\Omega^2 + r^2\delta^2}}}, \tag{C.12}$$

$$\tan\phi = \frac{r\sin(\varphi/2)}{\mu}. \tag{C.13}$$

The solution of equation (C.10) can be easily found

$$\theta(x) = \frac{2x}{L}\theta\left(\frac{L}{2}\right), \qquad 0 \le x \le \frac{L}{2}. \tag{C.14}$$

The solution of equation (C.9) can be simplified due to the existence of the first integral

$$\frac{\lambda^2}{2}\left(\frac{\partial}{\partial x}\theta\right)^2 + \cos(\theta - \phi) = 1. \tag{C.15}$$

The constant of integration on the right-hand side of (C.15) has been found from the boundary condition (C.11), which demands $\theta \to \phi$ then $x \to \infty$. Further integration in (C.15) for $L/2 \le x < \infty$ gives

$$\theta = \phi + 4\arctan\left(C_2 \exp\left(-\frac{x - L/2}{\lambda}\right)\right), \tag{C.16}$$

where C_2 is an integration constant, which should be determined from the matching conditions at $x = L/2$. For C_2 they give

$$(\phi + 4\arctan(C_2)) = -\frac{2C_2}{1 + C_2^2}\frac{L}{\lambda}. \tag{C.17}$$

Assuming additionally that γ_{BM} is not too small, namely that $L \ll \xi_N \min(1, \sqrt{\gamma_{BM}})$, from (C.17) it is easy to get

$$C_2 = -\tan\left(\frac{\phi}{4} - \frac{L}{4\lambda}\sin\frac{\phi}{2}\right), \tag{C.18}$$

resulting in

$$\theta(x) = \frac{2x}{\lambda}\sin\frac{\phi}{2}, \qquad 0 \le x \le \frac{L}{2}. \tag{C.19}$$

From (C.19) it follows that in the weak link region $|x| \le L/2$

$$U_N = \frac{2x}{\lambda}\mu\sin\frac{\phi}{2}, \qquad G_N = \frac{\Omega}{\mu}, \tag{C.20}$$

while under the S electrode, $L/2 \le x < \infty$

$$U_N = \mu\tan(\phi - 4\arctan(u)),$$
$$u = \tan\left(\frac{\phi}{4} - \frac{L}{4\lambda}\sin\frac{\phi}{2}\right)\exp\left(-\frac{x - L/2}{\lambda}\right). \tag{C.21}$$

Substitution of (C.7), (C.20) into expression (5) for the supercurrent in the N channel results in

$$\frac{2eI_N(\varphi)}{\pi TWd_N} = \frac{2}{\rho_N\xi_N\sqrt{\gamma_{BM}}} \times \sum_{\omega=-\infty}^{\infty}\frac{r^2\delta^2\sin\varphi\sqrt{(\Omega\gamma_{BM} + G_S)}}{\sqrt{2\Omega\mu^2(\sqrt{\Omega^2 + r^2\delta^2} + \mu)}}. \tag{C.22}$$

Appendix D. Solution in ferromagnet layer of RTO junction

The spatial distributions of the even and odd parts of $\Phi_F(x, z)$ in coordinate x can be found in the form of the superposition of superconducting correlations induced into the F film from superconductors and from the N part of the weak link. It has the same form as in (B.8) and (B.9)

$$R_F = \frac{\sqrt{\tilde\Omega}G_S\Delta\cos(\varphi/2)}{\Omega\gamma_{BF}}\frac{\cosh(\sqrt{\tilde\Omega}\frac{x}{\xi_F})}{\sinh(\sqrt{\tilde\Omega}\frac{L}{2\xi_F})} + \frac{\sqrt{\tilde\Omega}G_N R_N}{\Omega\gamma_{BFN}}\frac{\cosh(\sqrt{\tilde\Omega}\frac{z}{\xi_F})}{\sinh(\sqrt{\tilde\Omega}\frac{d_F}{\xi_F})}, \tag{D.1}$$

$$U_F = \frac{\sqrt{\tilde\Omega}G_N U_N}{\Omega\gamma_{BFN}}\frac{\cosh(\sqrt{\tilde\Omega}\frac{z}{\xi_F})}{\sinh(\sqrt{\tilde\Omega}\frac{d_F}{\xi_F})} - \frac{\tilde\Omega^{3/2}\xi_F^2 G_N(U_N/x)}{\Omega\gamma_{BFN}d_F} \times \sum_{n=-\infty}^{\infty}\frac{(-1)^n\cos(\frac{\pi n z}{d_F})\sinh(\kappa_n\frac{x}{\xi_F})}{\kappa_n^3\cosh(\kappa_n\frac{L}{2\xi_F})} + \frac{\sqrt{\tilde\Omega}G_S\delta\sin(\varphi/2)}{\Omega\gamma_{BF}}\frac{\sinh(\sqrt{\tilde\Omega}\frac{x}{\xi_F})}{\cosh(\sqrt{\tilde\Omega}\frac{L}{2\xi_F})}, \tag{D.2}$$

with the functions R_N, G_N, and U_N defined by equations following from the solution of the boundary problem in the N-layer described in appendix C.

$$R_N = r\Delta\cos(\varphi/2), \qquad G_N = \frac{\Omega}{\sqrt{\Omega^2 + r^2\delta^2\cos^2(\varphi/2)}}, \tag{D.3}$$

$$U_N = \alpha\Delta\sin(\varphi/2)\frac{G_S}{G_N}\frac{x}{\xi_N}, \qquad \alpha = \frac{2\sqrt{\Omega^2 + \delta^2}}{\sqrt{2(\sqrt{\Omega^2 + r^2\delta^2} + \mu)}}\frac{r}{\sqrt{1 - r}}. \tag{D.4}$$

The substitution of (D.1)–(D.4) into expression (5) gives that the supercurrent across the F-layer in the RTO junction

consists of the sum of $I_F(\varphi)$ and $I_{FN}(\varphi)$, where $I_F(\varphi)$ is the current through the one-dimensional double-barrier SFS structure defined by equation (B.11), while $I_{FN}(\varphi) = I_1(\varphi) + I_2(\varphi)$ has the form

$$\frac{2eI_1(\varphi)}{\pi TWd_F} = \frac{\Delta^2 \sin(\varphi)}{\rho_F d_F} \frac{\xi_F}{\gamma_{BF}\gamma_{BFN}\xi_N} \sum_{\omega=-\infty}^{\infty} \frac{\alpha G_S^2}{\tilde{\Omega}^2\omega^2}\Psi_1,$$
$$\Psi_1 = \frac{\sqrt{\tilde{\Omega}}}{\sinh(q_L)} - \frac{2\tilde{\Omega}}{\sinh(2q_L)}, \tag{D.5}$$

$$\frac{2eI_2(\varphi)}{\pi TWd_F} = \frac{\Delta^2 \sin(\varphi)}{\rho_F d_F} \frac{1}{\gamma_{BFN}} \sum_{\omega=-\infty}^{\infty} \frac{rG_N G_S}{\omega^2\tilde{\Omega}^2} \times \left(\frac{\alpha}{\gamma_{BFN}\xi_N}\Psi_2 + \frac{\tilde{\Omega}}{\gamma_{BF}\cosh q_L}\right),$$
$$\Psi_2 = \frac{d_F\tilde{\Omega}(2q_d + \sinh(2q_d))}{4q_d\sinh^2(q_d)} - \frac{\tilde{\Omega}\xi_F}{q_d\cosh(q_L)} - \sum_{n=1}^{\infty} \frac{2\tilde{\Omega}^3\xi_F}{q_d\kappa_n^4\cosh(\frac{L\kappa_n}{2\xi_F})}. \tag{D.6}$$

Application of conditions (B.14) allows one to neglect some terms in $I_{FN}(\varphi) = I_{FN1}(\varphi) + I_{FN2}(\varphi) + I_{FN3}(\varphi)$ and to simplify the remaining terms, leading to the following expressions:

$$\frac{2eI_{FN1}(\varphi)}{\pi TWd_F} = \frac{\Delta^2 \sin(\varphi)}{\gamma_{BF}\gamma_{BFN}\rho_F d_F} \frac{\xi_F}{\xi_N} \sum_{\omega=-\infty}^{\infty} \frac{\alpha G_S^2}{\omega^2\tilde{\Omega}^2} \frac{\sqrt{\tilde{\Omega}}}{\sinh q_L}, \tag{D.7}$$

$$\frac{2eI_{FN2}(\varphi)}{\pi TWd_F} = \frac{\Delta^2 \sin(\varphi)}{2\gamma_{BFN}^2\rho_F d_F} \sum_{\omega=-\infty}^{\infty} \frac{r\alpha G_N G_S}{\omega^2\tilde{\Omega}^{3/2}} \frac{\xi_F}{\xi_N}, \tag{D.8}$$

$$\frac{2eI_{FN3}(\varphi)}{\pi TWd_F} = \frac{\Delta^2 \sin(\varphi)}{\gamma_{BFN}\gamma_{BF}\rho_F d_F} \sum_{\omega=-\infty}^{\infty} \frac{rG_N G_S}{\omega^2\tilde{\Omega}} \frac{1}{\cosh q_L}. \tag{D.9}$$

References

[1] Likharev K K 1979 *Rev. Mod. Phys.* **51** 101
[2] Golubov A A, Kupriyanov M Yu and Il'ichev E 2004 *Rev. Mod. Phys.* **76** 411
[3] Buzdin A I 2005 *Rev. Mod. Phys.* **77** 935
[4] Bergeret F S, Volkov A F and Efetov K B 2005 *Rev. Mod. Phys.* **77** 1321
[5] Ryazanov V V, Oboznov V A, Rusanov A Yu, Veretennikov A V, Golubov A A and Aarts J 2001 *Phys. Rev. Lett.* **86** 2427
[6] Frolov S M, Van Harlingen D J, Oboznov V A, Bolginov V V and Ryazanov V V 2004 *Phys. Rev.* B **70** 144505
[7] Kontos T, Aprili M, Lesueur J, Genet F, Stephanidis B and Boursier R 2002 *Phys. Rev. Lett.* **89** 137007
[8] Sellier H, Baraduc C, Lefloch F and Calemczuck R 2003 *Phys. Rev.* B **68** 054531
[9] Blum Y, Tsukernik A, Karpovski M and Palevski A 2004 *Phys. Rev.* B **70** 214501
[10] Surgers C, Hoss T, Schonenberger C and Strunk C 2002 *J. Magn. Magn. Mater.* **240** 598
[11] Bell C, Loloee R, Burnell G and Blamire M G 2005 *Phys. Rev.* B **71** 180501(R)
[12] Frolov S M, Van Harlingen D J, Bolginov V V, Oboznov V A and Ryazanov V V 2006 *Phys. Rev.* B **74** 020503
[13] Oboznov V A, Bol'ginov V V, Feofanov A K, Ryazanov V V and Buzdin A I 2006 *Phys. Rev. Lett.* **96** 197003
[14] Shelukhin V *et al* 2006 *Phys. Rev.* B **73** 174506
[15] Weides M, Tillmann K and Kohlstedt H 2006 *Physica* C **437/438** 349
[16] Weides M, Kemmler M, Kohlstedt H, Buzdin A, Goldobin E, Koelle D and Kleiner R 2006 *Appl. Phys. Lett.* **89** 122511
[17] Weides M, Kemmler M, Kohlstedt H, Waser R, Koelle D, Kleiner R and Goldobin E 2006 *Phys. Rev. Lett.* **97** 247001
[18] Pfeiffer J, Kemmler M, Koelle D, Kleiner R, Goldobin E, Weides M, Feofanov A K, Lisenfeld J and Ustinov A V 2008 *Phys. Rev.* B **77** 214506
[19] Sellier H, Baraduc C, Lefloch F and Calemczuck R 2004 *Phys. Rev. Lett.* **92** 257005
[20] Born F, Siegel M, Hollmann E K, Braak H, Golubov A A, Gusakova D Yu and Kupriyanov M Yu 2006 *Phys. Rev.* B **74** 140501
[21] Robinson J W A, Piano S, Burnell G, Bell C and Blamire M G 2006 *Phys. Rev. Lett.* **97** 177003
[22] Piano S, Robinson J W A, Burnell G and Blamire M G 2007 *Eur. Phys. J.* B **58** 123
[23] Robinson J W, Piano S, Burnell G, Bell C and Blamire M G 2007 *Phys. Rev.* B **76** 094522
[24] Keizer R S, Goennenwein S T B, Klapwijk T M, Miao G, Xiao G and Gupta A 2006 *Nature* **439** 825
[25] Khaire T S, Khasawneh M A, Pratt W P Jr and Birge N O 2010 *Phys. Rev. Lett.* **104** 137002
[26] Robinson J W A, Witt J D S and Blamire M G 2010 *Science* **329** 59
[27] Wang J, Singh M, Tian M, Kumar N, Liu B, Shi C, Jain J K, Samarth N, Mallouk T E and Chan M H W 2010 *Nature Phys.* **6** 389
[28] Anwar M S, Czeschka F, Hesselberth M, Porcu M and Aarts J 2010 *Phys. Rev.* B **82** 100501(R)
[29] Anwar M S, Veldhorst M, Brinkman A and Aarts J 2012 *Appl. Phys. Lett.* **100** 052602
[30] Ortlepp T, Ariando, Mielke O, Verwijs C J M, Foo K F K, Rogalla H, Uhlmann F H and Hilgenkamp H 2006 *Science* **312** 1495
[31] Feofanov A K *et al* 2010 *Nature Phys.* **6** 593
[32] Ustinov A V and Kaplunenko V K 2003 *J. Appl. Phys.* **94** 5405
[33] Mints R G 1998 *Phys. Rev.* B **57** R3221
[34] Buzdin A and Koshelev A E 2003 *Phys. Rev.* B **67** 220504
[35] Pugach N G, Goldobin E, Kleiner R and Koelle D 2010 *Phys. Rev.* B **81** 104513
[36] Yu Kupriyanov M, Golubov A A and Siegel M 2006 *Proc. SPIE* **6260** 62600S
[37] Goldobin E, Koelle D, Kleiner R and Mints R G 2011 *Phys. Rev. Lett.* **107** 227001
[38] Sickinger H, Lipman A, Weides M, Mints R G, Kohlstedt H, Koelle D, Kleiner R and Goldobin E 2012 *Phys. Rev. Lett.* **109** 107002
[39] Lipman A, Mints R G, Kleiner R, Koelle D and Goldobin E 2012 arXiv:1207.3013
[40] Koshelev A E 2012 arXiv:1209.5438
[41] Goldobin E, Koelle D, Kleiner R and Buzdin A 2007 *Phys. Rev.* B **76** 224523
[42] Klenov N V, Pugach N G, Sharafiev A V, Bakurskiy S V and Kornev V K 2010 *Phys. Solid State* **52** 2246
[43] Vasenko A S, Golubov A A, Kupriyanov M Yu and Weides M 2008 *Phys. Rev.* B **77** 134507
[44] Vasenko A S, Kawabata S, Golubov A A, Kupriyanov M Yu, Lacroix C and Hekking F W J 2011 *Phys. Rev.* B **84** 024524
[45] Konschelle F, Cayssol J and Buzdin A I 2008 *Phys. Rev.* B **78** 134505
[46] Houzet M, Vinokur V and Pistolesi F 2005 *Phys. Rev.* B **72** 220506

[47] Karminskaya T Yu and Kupriyanov M Yu 2007 *Pis. Zh. Eksp. Teor. Fiz.* **85** 343
Karminskaya T Yu and Kupriyanov M Yu 2007 *JETP Lett.* **85** 286 (Engl. transl.)
[48] Karminskaya T Yu and Kupriyanov M Yu 2007 *Pis. Zh. Eksp. Teor. Fiz.* **85** 343
Karminskaya T Yu and Kupriyanov M Yu 2007 *JETP Lett.* **86** 61 (Engl. transl.)
[49] Karminskaya T Yu, Kupriyanov M Yu and Golubov A A 2008 *Pis. Zh. Eksp. Teor. Fiz.* **87** 657
Karminskaya T Yu, Kupriyanov M Yu and Golubov A A 2008 *JETP Lett.* **87** 570 (Engl. transl.)
[50] Karminskaya T Yu, Golubov A A, Kupriyanov M Yu and Sidorenko A S 2009 *Phys. Rev.* B **79** 214509
[51] Karminskaya T Yu, Golubov A A, Kupriyanov M Yu and Sidorenko A S 2010 *Phys. Rev.* B **81** 214518
[52] Bakurskiy S V, Klenov N V, Karminskaya T Yu, Kupriyanov M Yu and Kornev V K 2012 *Solid State Phenom.* **190** 401
[53] Bergeret F S, Volkov A F and Efetov K B 2001 *Phys. Rev. Lett.* **86** 3140
[54] Fominov Ya V, Chtchelkatchev N M and Golubov A A 2002 *Phys. Rev.* B **66** 014507
[55] Furusaki A and Tsukada M 1991 *Solid State Commun.* **78** 299
[56] Furusaki A and Tsukada M 1991 *Phys. Rev.* B **43** 164
[57] Ivanov Z G, Kupriyanov M Yu, Likharev K K, Meriakri S V and Snigirev O V 1981 *Fiz. Nizk. Temp.* **7** 560
Ivanov Z G, Kupriyanov M Yu, Likharev K K, Meriakri S V and Snigirev O V 1981 *Sov. J. Low Temp. Phys.* **7** 274 (Engl. transl.)
[58] Zubkov A A and Kupriyanov M Yu 1983 *Fiz. Nizk. Temp.* **9** 548
Zubkov A A and Kupriyanov M Yu 1983 *Sov. J. Low Temp. Phys.* **9** 279 (Engl. transl.)
[59] Kupriyanov M Yu 1992 *Pis. Zh. Eksp. Teor. Fiz.* **56** 414
Kupriyanov M Yu 1992 *JETP Lett.* **56** 399 (Engl. transl.)
[60] Demler E A, Arnold G B and Beasley M R 1997 *Phys. Rev.* B **55** 15174
[61] Usadel K D 1970 *Phys. Rev. Lett.* **25** 507
[62] Kuprianov M Yu and Lukichev V F 1988 *Zh. Eksp. Teor. Fiz.* **94** 139
Kuprianov M Yu and Lukichev V F 1988 *Sov. Phys.—JETP* **67** 1163 (Engl. transl.)
[63] Chtchelkatchev N M and Burmistrov I S 2003 *Phys. Rev.* B **68** 140501(R)
[64] Burmistrov I S and Chtchelkatchev N M 2005 *Phys. Rev.* B **72** 144520
[65] Champel T and Eschrig M 2005 *Phys. Rev.* B **72** 054523
[66] Houzet M and Buzdin A I 2006 *Phys. Rev.* B **74** 214507
[67] Maleki M A and Zareyan M 2006 *Phys. Rev.* B **74** 144512
[68] Fominov Y V, Volkov A F and Efetov K B 2007 *Phys. Rev.* B **75** 104509
[69] Volkov A F and Anishchanka A 2005 *Phys. Rev.* B **71** 024501
[70] Volkov A F and Efetov K B 2008 *Phys. Rev.* B **78** 024519
[71] Crouzy B, Tollis S and Ivanov D A 2007 *Phys. Rev.* B **76** 134502
[72] Golubov A A, Kupriyanov M Yu and Fominov Ya V 2002 *Pis. Zh. Eksp. Teor. Fiz.* **75** 588
Golubov A A, Kupriyanov M Yu and Fominov Ya V 2002 *JETP Lett.* **75** 709 (Engl. transl.)
[73] Buzdin A 2003 *Pis. Zh. Eksp. Teor. Fiz.* **78** 1073
Buzdin A 2003 *JETP Lett.* **78** 583 (Engl. transl.)
[74] Kupriyanov M Yu, Lukichev V F and Orlikovskii A A 1986 *Mikroelektronika* **15** 328
Kupriyanov M Yu, Lukichev V F and Orlikovskii A A 1986 *Sov. Microelectron.* **15** 185 (Engl. transl.)